Phosphorus-Mediated Gold Aggregation on a Metal Cluster: Syntheses, Structures, Dynamic Behavior, and Ligand Addition Reactions of the Clusters $(\mu\text{-H})_n Fe_3(CO)_9P[Au(PR_3)]_{3-n}$ (n = 0, 1, 2)

Deborah L. Sunick, Peter S. White, and Cynthia K. Schauer*

Department of Chemistry, The University of North Carolina at Chapel Hill, Chapel Hill, North Carolina 27599-3290

Received July 2, 1993®

The phosphorus heteroatom in the cluster $[H_2Fe_3(CO)_9P]^-$ has a high affinity for $(R_3P)Au^+$ fragments, permitting the synthesis of a series of gold-substituted clusters, $(\mu\text{-H})_nFe_3(CO)_9P[Au(PR_3)]_{3-n}$ (n = 0, 1, 2). Reactions between $(R_3P)AuCl$ (R = Ph, Et) and the silylphosphinidene cluster $(\mu\text{-H})_2Fe_3(CO)_9[\mu_3\text{-PSi}(i\text{-Pr})_3]$ (**1**) (with evolution of $(i\text{-Pr})_3SiCl$) or the desilylated anion $[(\mu\text{-H})Fe_3(CO)_9(\mu_3\text{-PH})]^-$ (**2**) serve as the synthetic routes to these clusters. Coordination of the first $(R_3P)Au^+$ fragment occurs at the terminal position on the phosphorus atom to yield $(\mu\text{-H})_2Fe_3(CO)_9P[Au(PR_3)]$ (**3a**, R = Ph; **3b**, R = Et). This initial μ_3-$PAu(PR_3)$ interaction serves as a "nucleation" site for coordination of additional Au(I) fragments to yield the Au_2 clusters $(\mu\text{-H})Fe_3(CO)_9P\{[Au(PR_3)][Au(PR'_3)]\}$ (**4a**, R = R′ = Ph; **4b**, R = R′ = Et; **4c**, R = Ph, R′ = Et) and the Au_3 clusters $Fe_3(CO)_9P[Au(PR_3)]_3$ (**5a**, R = Ph; **5b**, R = Et). Single-crystal X-ray structure determinations show that the Au_2 cluster **4a** contains a coordinated $[Au_2(PPh_3)_2]^{2+}$ fragment while the Au_3 cluster **5a** contains a coordinated triangular $[Au_3(PPh_3)_3]^{3+}$ unit. The variable-temperature ^{31}P NMR spectra for the Au_2 clusters were analyzed to yield activation parameters for a fluxional process that equilibrates the gold-bound phosphine ligands at room temperature. Both **3a** and **4a** coordinate an additional PPh_3 ligand at low temperature, and an analysis of the temperature dependence of the equilibrium constant for **4a** yields $\Delta H° = -7.6(2)$ kcal mol^{-1} and $\Delta S° = -25.0(7)$ cal mol^{-1} K^{-1} for the PPh_3 addition reaction. Crystal data for **4a**·1.5C_6H_6 at 298 K: Monoclinic, $C2/c$, a = 20.422(9) Å, b = 15.434(6) Å, c = 34.135(11) Å, β = 93.29(3)°, Z = 8. Crystal data for **5a**·0.3CH_2Cl_2·0.7Et_2O at 123 K: Monoclinic, $P2_1/n$, a = 16.260(11) Å, b = 20.363(7) Å, c = 19.526(5) Å, β = 93.45(5), Z = 4.

Introduction

Interactions between the metal centers in formally closed-shell d^{10} complexes influence the structures adopted by the complexes as well as their chemical and physical properties.[1] A readily apparent example of these interactions is the tendency of two-coordinate Au(I) complexes to form dimers, chains, or layered structures in the solid state.[1] The Au···Au contacts in these structures are ~3.0 Å, similar to that observed in metallic gold (2.884 Å). The energetics of a Au(I)–Au(I) interaction for a binuclear molecular complex in solution was recently shown to be of the same magnitude as a hydrogen bond (7–8 kcal mol^{-1});[2] thus it is not surprising that these interactions play a significant role in determining structure. An accurate description of Au···Au bonding requires inclusion of relativistic effects,[3] which are at a maximum for gold among the transition metals.

Attractive interactions between Au(I) ions have facilitated the preparation of a variety of molecular complexes. Included among these is a remarkable series of heteroatom-centered gold clusters, $L[Au(PR_3)]_n^{m+}$ (L = C, n = 5 and 6;[4] L = N, n = 5;[5] L = P, n = 5 and 6[6]), that have recently been reported by Schmidbaur and co-workers. The interactions between gold ions in these clusters are responsible for the formation of the hypercoordinate center atom.[7] Additionally, interactions between d^{10}-$[(PR_3)Au]^+$ fragments and transition metal clusters have been examined to explore the isolobal analogy between a $Au(PR_3)$ fragment and a hydrogen atom.[8] In the vast majority of cases, a single $Au(PR_3)$ fragment will adopt the same coordination site as the cluster-bound hydrogen atom it replaced. When more than one hydrogen atom is replaced, however, the isolobal analogy breaks down due to the favored formation of Au···Au interactions.[8] Homo- and heterometallic d^{10}–d^{10} interactions have also been observed between other coinage metal cations (Cu^+, Ag^+) bound to transition metal clusters.[9]

We have prepared a series of gold-substituted transition metal clusters that result from sequential aggregation of one to three gold(I) complexes about the phosphorus heteroatom in the cluster $[(H)_nFe_3(CO)_9P]^{(3-n)-}$, similar to the phosphorus-centered clusters described above. Reported herein is a comprehensive study of the syntheses, structures, dynamics, and ligand addition reactions of the gold-substituted clusters $(\mu\text{-H})_nFe_3(CO)_9P[Au(PR_3)]_{3-n}$ (n = 0, 1, 2). The cluster-bound phosphorus atom provides a sensitive NMR probe of changes at the gold sites in this series of clusters.

Experimental Section

General Methods. All manipulations were performed under an inert atmosphere of nitrogen using standard Schlenk-line techniques. Toluene,

* Abstract published in *Advance ACS Abstracts*, November 1, 1993.

(1) Jansen, M. *Angew. Chem., Int. Ed. Engl.* **1987**, *26*, 1098.
(2) Schmidbaur, H.; Graf, W.; Müller, G. *Angew. Chem., Int. Ed. Engl.* **1988**, *27*, 417.
(3) Pyykkö, P.; Desclaux, J.-P. *Acc. Chem. Res.* **1979**, *12*, 276.
(4) (a) Scherbaum, F.; Grohmann, A.; Huber, B.; Krüger, C.; Schmidbaur, H. *Angew. Chem., Int. Ed. Engl.* **1988**, *27*, 1544. (b) Scherbaum, F.; Grohmann, A.; Müller, G.; Schmidbaur, H. *Angew. Chem., Int. Ed. Engl.* **1989**, *28*, 463. (c) Steigelmann, O.; Bissinger, P.; Schmidbaur, H. *Angew. Chem., Int. Ed. Engl.* **1990**, *29*, 1399.
(5) Grohmann, A.; Riede, J.; Schmidbaur, H. *Nature* **1990**, *345*, 140.
(6) (a) Schmidbaur, H.; Weidenhiller, G.; Steigelmann, O. *Angew. Chem., Int. Ed. Engl.* **1991**, *30*, 433. (b) Zeller, E.; Schmidbaur, H. *J. Chem. Soc., Chem. Commun.* **1993**, 69.
(7) Görling, A.; Rösch, N.; Ellis, D. E.; Schmidbaur, H. *Inorg. Chem.* **1991**, *30*, 3986.
(8) (a) Hall, K. P.; Mingos, D. M. P. *Prog. Inorg. Chem.* **1984**, *32*, 237. (b) Salter, I. D. *Adv. Organomet. Chem.* **1989**, *29*, 249.
(9) See, for example: (a) Freeman, M. J.; Orpen, A. G.; Salter, I. D. *J. Chem. Soc., Dalton Trans.* **1987**, 1001. (b) Freeman, M. J.; Orpen, A. G.; Salter, I. D. *J. Chem. Soc., Dalton Trans.* **1987**, 379. (c) Brice, R. A.; Pearse, S. C.; Salter, I. D.; Henrick, K. *J. Chem. Soc., Dalton Trans.* **1986**, 2181. (d) Brown, S. S. D.; Salter, I. D.; Smith, B. M. *J. Chem. Soc., Chem. Commun.* **1985**, 1439. (e) Freeman, M. J.; Green, M.; Orpen, A. G.; Salter, I. D. Stone, F. G. A. *J. Chem. Soc., Chem. Commun.* **1983**, 1332.

0020-1669/93/1332-5665$04.00/0 © 1993 American Chemical Society

pentane, benzene, diethyl ether, and hexanes were distilled from sodium benzophenone ketyl, dichloromethane was distilled from P_4O_{10}, and triethylamine (Aldrich) was distilled from CaH_2. Triphenylphosphine (Aldrich), triethylphosphine, chloro(triphenylphosphine)gold(I) (Strem Chemicals, Aldrich), chloro(triethylphosphine)gold (I) (Strem Chemicals), 1,8-diazabicyclo[5.4.0]undec-7-ene (Aldrich), and Kieselgel-60 (Fluka) were used as received. The silylphosphinidene cluster $(\mu\text{-H})_2Fe_3(CO)_9[\mu_3\text{-PSi}(i\text{-Pr})_3]$ and $[(\mu\text{-H})Fe_3(CO)_9(\mu_3\text{-PH})]^-$ were prepared by following published procedures.[10]

Infrared spectra were recorded on a Bomem Michelson 120 Fourier transform infrared spectrometer. Proton NMR spectra were recorded either on a Bruker AC-200, a Bruker WM-250, or a Bruker AMX-300 spectrometer. All chemical shifts were reported as positive if downfield from Me_4Si and were referenced to residual protons in the solvent. Room-temperature ^{31}P NMR spectra were recorded on the same instruments operating at 81, 101, and 121 MHz, respectively. The chemical shifts were referenced to an external $P(OCH_3)_3$ sample (δ 140.0 ppm) by the sample replacement method. The low-temperature ^{31}P NMR spectra were recorded on the Bruker AMX-300 spectrometer, and the temperature of the probe was calibrated using a methanol insert.[11] The low-temperature ^{13}C NMR spectra were recorded on the Bruker AMX-300 spectrometer operating at 75 MHz, and the chemical shifts were referenced to CD_2Cl_2 (δ 53.8 ppm). The program DNMR3 was utilized to obtain rate constants by fitting the variable-temperature spectra.[12] Elemental analyses were performed by Pascher Microanalytical Laboratories (Remagen, Germany) and Oneida Research Services (Whitesboro, New York).

Preparations. **$(\mu\text{-H})_2Fe_3(CO)_9P[Au(PPh_3)]$ (3a).** A mixture of $(\mu\text{-H})_2Fe_3(CO)_9[\mu_3\text{-PSi}(i\text{-Pr})_3]$ (**1**) (240 mg, 0.39 mmol) and $(Ph_3P)AuCl$ (200 mg, 0.40 mmol) in 10 mL of CH_2Cl_2 was stirred for 3–4 h. Infrared spectroscopy showed nearly quantitative conversion to **3a**. The solvent was removed under reduced pressure, and the residue was purified by chromatographic separation at 233 K (Kieselgel 60). Elution yielded green $Fe_3(CO)_{12}$ (from trace impurities in **1**, hexanes/CH_2Cl_2, 3:1), brown **3a** (hexanes/CH_2Cl_2, 1:1), and red **4a** (hexanes/CH_2Cl_2, 1:1). Crystallization of the **3a** fraction from a solution of 4:1 hexanes/Et_2O at 213 K yielded crystalline red-brown **3a** (57 mg, 16%). The low isolated yield is due to product loss during chromatography. Anal. Calcd (found) for $C_{27}H_{17}O_9AuFe_3P_2$: C, 35.56 (35.88); H, 1.88 (1.99).

$(\mu\text{-H})_2Fe_3(CO)_9P[Au(PEt_3)]$ (3b). Compound **3b** was prepared as described for **3a** from **1**. Yield: 57 mg (24%). Anal. Calcd (found) for $C_{15}H_{17}O_9AuFe_3P_2$: C, 23.47 (21.72); H, 2.23 (1.99).

$(\mu\text{-H})Fe_3(CO)_9P[Au(PPh_3)]_2$ (4a). To a mixture of **1** (59 mg, 0.097 mmol) and $(Ph_3P)AuCl$ (81 mg, 0.16 mmol, 1.7 equiv) in 20 mL of CH_2Cl_2 was added NEt_3 (6 μL, 0.04 mmol). Infrared spectroscopy showed immediate conversion of **1** to **4a**. The solvent and volatiles were removed under reduced pressure, and the residue was purified by chromatographic separation (Kieselgel 60). Elution with hexanes/CH_2Cl_2 (3:1) yielded dark red **4a**. Slow diffusion of pentane into an Et_2O solution of **4a** yielded a deep red crystalline solid (43 mg, 34%). Anal. Calcd (found) for $C_{45}H_{31}O_9Au_2Fe_3P_3$: C, 39.45 (38.67); H, 2.28 (2.24).

$(\mu\text{-H})Fe_3(CO)_9P[Au(PEt_3)]_2$ (4b). Compound **4b** was prepared as described for **4a**. Yield: 46 mg (17%). Anal. Calcd (found) for $C_{21}H_{31}O_9Au_2Fe_3P_3$: C, 23.32 (23.61); H, 2.89 (2.77).

$(\mu\text{-H})Fe_3(CO)_9P\{[Au(PEt_3)][Au(PPh_3)]\}$ (4c). An NMR tube was charged with **4a** (10.08 mg, 0.0074 mmol), **4b** (7.86 mg, 0.0073 mmol), and CD_2Cl_2. The $^{31}P\{^1H\}$ NMR spectrum showed **4c** in addition to the starting clusters in approximately a 1:2:1 (**4a**:**4c**:**4b**) ratio. The three clusters eluted together as a single red band by chromatography (Kieselgel-60, 233 K).

$Fe_3(CO)_9P[Au(PPh_3)]_3$ (5a). To a mixture of **1** (62 mg, 0.10 mmol) and $(Ph_3P)AuCl$ (150 mg, 0.30 mmol) in 20 mL of CH_2Cl_2 was added NEt_3 (25 μL, 0.18 mmol). After stirring overnight, the volatiles were removed under reduced pressure. The residue was dissolved in a minimum amount of CH_2Cl_2, filtered, and layered with Et_2O to yield dark red crystalline **5a** (157 mg, 28%). Anal. Calcd (found) for $C_{63}H_{45}O_9Au_3Fe_3P_4$: C, 41.39 (41.57); H, 2.48 (2.07).

$Fe_3(CO)_9P[Au(PEt_3)]_3$ (5b). Compound **5b** was prepared as described for **5a**. Yield: 237 mg (33%). Anal. Calcd (found) for $C_{27}H_{45}O_9Au_3Fe_3P_4$: C, 23.23 (23.31); H, 3.25 (3.14).

$(\mu\text{-H})[\mu\text{-Au}(PPh_3)]Fe_3(CO)_9(\mu_3\text{-PPh})$. The monogold-substituted phenylphosphinidene cluster was synthesized by a variation of a published route as described here.[13] To a flask charged with $(\mu\text{-H})_2Fe_3(CO)_9(\mu_3\text{-PPh})$ (113 mg, 0.21 mmol) and $(Ph_3P)AuCl$ (93 mg, 0.19 mmol) was added 20 mL of CH_2Cl_2. After the solution was stirred for 2 days, the solvent and volatiles were removed under reduced pressure, the residue was extracted in 3 mL of a CH_2Cl_2/hexanes (2:3) solution, and the extract purified by column chromatography on Florisil. Elution with CH_2Cl_2/hexanes (1:1) yielded brown $(\mu\text{-H})_2Fe_3(CO)_9(\mu_3\text{-PPh})$ (hexanes) followed by red $(\mu\text{-H})[\mu\text{-Au}(PPh_3)]Fe_3(CO)_9(\mu_3\text{-PPh})$. Removal of the solvent from the red fraction yielded pure $(\mu\text{-H})[\mu\text{-Au}(PPh_3)]Fe_3(CO)_9(\mu_3\text{-PPh})$ (25 mg, 17%). IR (ν_{CO}, cm^{-1}; hexanes): 2093 (w), 2062 (m), 2031 (vs), 2002 (s), 1991 (m), 1970 (w), 1937 (vw). $^{31}P\{^1H\}$ NMR (δ, ppm, C_6D_6): 357.1 (br, μ-*P*), 55.1 (d, $^2J_{PP}$ = 38 Hz, Au*P*). ^1H NMR (δ, ppm, CD_2Cl_2): 8.02, 7.50, 7.30 (m, μ_3-P(C_6H_5), AuP(C_6H_5)), –23.30 (d, $^2J_{PH}$ = 34.3 Hz, μ-*H*). Anal. Calcd (found) for $C_{33}H_{21}O_9AuFe_3P_2$: C, 40.12 (40.98); H, 2.14 (2.27).

Reaction of 3a and PPh_3. A sample containing **3a** (14.0 mg, 0.015 mmol), PPh_3 (8.0 mg, 0.030 mmol, 2 equiv), and CD_2Cl_2 (510 μL) was prepared in a 5-mm NMR tube for analysis by NMR spectroscopy.

Reaction of 4a and PPh_3. A sample containing **4a** (21.0 mg, 0.015 mmol), PPh_3 (8.0 mg, 0.030 mmol, 2 equiv), and CD_2Cl_2 (510 μL) was prepared in a 5-mm NMR tube for analysis by NMR spectroscopy. $^{31}P\{^1H\}$ NMR analysis of the mixture at 170 K showed quantitative formation of the adduct **4a**·PPh_3. The concentrations of the clusters **4a** and **4a**·PPh_3 as a function of temperature were determined by monitoring the chemical shift of the cluster-bound phosphorus atom (P_c) and solving the equation $\delta_{obs}(T) = N(\mathbf{4a}\cdot PPh_3)\cdot\delta(\mathbf{4a}\cdot PPh_3) + N(\mathbf{4a})\cdot\delta(\mathbf{4a})$, where $N(x)$ denotes the mole fraction of x, $N(\mathbf{4a}) + N(\mathbf{4a}\cdot PPh_3) = 1$, $\delta(\mathbf{4a}\cdot PPh_3)$ is the chemical shift of the adduct measured in the slow-exchange limit at 170 K, and $\delta(\mathbf{4a})$ is the chemical shift of **4a** measured as a function of temperature in an experiment without PPh_3 present. The equilibrium constant was determined at each temperature over the range (217–272 K) by the following equation: K_{eq} = [(mol **4a**)(0.510 × 10^{-3} L)/[(mol PPh_3)(mol **4a**·PPh_3)]. A linear analysis of a plot of ln K_{eq} versus $1/T$ was analyzed to extract the enthalpy ($\Delta H°$) and entropy ($\Delta S°$) for the ligand addition reaction. The mole-ratio data derived above from analysis of the P_c chemical shift was used to successfully predict the chemical shift for the single PPh_3 resonance at T = 272 K.

Reaction of 5a and PPh_3. A sample containing **5a** (28.1 mg, 0.015 mmol), PPh_3 (8.1 mg, 0.030 mmol, 2 equiv), and CD_2Cl_2 (510 μL) was prepared in a 5-mm NMR tube for analysis by NMR spectroscopy.

Addition of PEt_3 to $(\mu\text{-H})_2Fe_3(CO)_9P[Au(PEt_3)]$. Upon the addition of PEt_3 (5.5 μL) to an NMR tube containing **3a** (approximately 10 mg) in CD_2Cl_2, the color changed immediately from brown to red. ^{31}P NMR analysis confirmed complete conversion of **3a** to **2**.

X-ray Structure Determinations. Crystallographic data and experimental parameters are summarized in Table I. The structures were solved using software from the NRCVAX computing package.[14] Least squares refinement on F minimized the function $\sum w(|F_o| - |F_c|)^2$.

$(\mu\text{-H})Fe_3(CO)_9P[Au(PPh_3)]_2$ (4a). Crystals suitable for analysis by X-ray diffraction were obtained by slow diffusion of pentane into an Et_2O solution of pure **4a**. The crystal was coated with an epoxy and mounted on the end of a glass fiber. Lattice parameters were determined by least squares refinement of the setting angles of 25 high-angle reflections (2θ = 33.36–37.52°). The room-temperature data collection was monitored by measurement of the intensities of three control reflections, which showed no significant intensity variation over the course of data collection. An empirical absorption correction was applied to the raw data utilizing the intensity profiles from ψ scan data (range of transmission factors 0.18-0.31). The phenyl rings were refined as rigid groups. The cluster crystallizes with a 1.5 molecules of benzene per cluster in the unit cell with the half-molecule of benzene located on a 2-fold axis parallel to *b*. All non-hydrogen atoms were refined anisotropically. The bridging hydride ligand was not observed in the final difference map. Hydrogen atoms were included in calculated positions. Final fractional atomic coordinates and thermal parameters may be found in Table II.

$Fe_3(CO)_9P[Au(PPh_3)]_3$ (5a). Crystals suitable for analysis by X-ray diffraction were obtained by slow diffusion of Et_2O into a CH_2Cl_2 solution of pure **5a**. The crystal was coated with Paratone N (Exxon),

(10) Sunick, D. L.; White, P. S.; Schauer, C. K. *Organometallics* **1993**, *12*, 245.
(11) VanGeet, A. L. *Anal. Chem.* **1970**, *42*, 679.
(12) *QCPE Bull.* **1970**, *11*, 165.
(13) (a) Deck, W.; Schwarz, M.; Vahrenkamp, H. *Chem. Ber.* **1987**, *120*, 1515. Vahrenkamp and co-workers suggest the formulation $(\mu\text{-H})(\mu\text{-AuPPh}_3)Fe_3(CO)_9(\mu_3\text{-PPh})$ for a minor product in their synthesis; spectroscopic data for $(\mu\text{-H})(\mu\text{-AuPPh}_3)Fe_3(CO)_9(\mu_3\text{-PPh})$ is reported in the Experimental Section. (b) Roland, E.; Fischer, K.; Vahrenkamp, H. *Angew. Chem., Int. Ed. Engl.* **1983**, *22*, 326.
(14) Gabe, E. J.; Le Page, Y.; Charland, J.-P.; Lee, F. L.; White, P. S. *J. Appl. Crystallogr.* **1989**, *22*, 384.

Table I. Crystallographic Experiments and Computations for $(\mu\text{-H})Fe_3(CO)_9P[Au(PPh_3)]_2$ (**4a**) and $Fe_3(CO)_9P[Au(PPh_3)]_3$ (**5a**)

	compd	
	4a·1.5C_6H_6	**5a**·0.3CH_2Cl_2·0.7Et_2O
formula	$C_{54}H_{40}Au_2Fe_3O_9P_3$	$C_{66.1}H_{52.6}Au_3Cl_{0.6}Fe_3O_{9.7}P_4$
fw	1486.28	1905.78
temp, K	298	123
space group	$C2/c$ (No. 15)	$P2_1/n$ (No. 14)
a, Å	20.422(9)	16.260(11)
b, Å	15.434(6)	20.363(7)
c, Å	34.135(11)	19.526(5)
α, deg	90	90
β, deg	93.29(3)	93.45(5)
γ, deg	90	90
V, Å^3	10 742(7)	6454(5)
Z	8	4
d_{calc}, g cm^{-3}	1.838	1.962
λ(Mo Kα), Å	0.709 30	0.709 30
μ(Mo Kα), cm^{-1}	63.2	76.1
T_{min}–T_{max}	0.181–0.306	0.075–0.179
R^a	0.048	0.077
R_w^b	0.060	0.101

$^a R = (\Sigma\|\|F_o| - |F_c\|\|)/\Sigma|F_o|$. $^b R_w = [\Sigma w(|F_o| - |F_c|)^2/\Sigma w(F_o)^2]^{1/2}$.

mounted on the end of a glass fiber, and cooled under a stream of N_2 at 123 K. Lattice parameters were determined by least squares refinement of the setting angles of 16 high-angle reflections (2θ = 20.09–31.93°). The data collection was monitored by measurement of the intensities of three control reflections, which showed no significant intensity variation over the course of data collection. An empirical absorption correction was applied to the raw data utilizing the intensity profiles from ψ scan data (range of transmission factors 0.075–0.18). The cluster crystallizes with a partial molecule of ether (refined to 70% occupancy) and a partial molecule of CH_2Cl_2 (refined to 30% occupancy) per cluster in the unit cell. Rotational disorder was observed in two phenyl rings and was modeled by refining the disordered rings as two concentric rings joined at the ipso and para carbon atoms (C(ipso):C111/C151, 48%/52%; C131/C141, 60%/40%). The remaining phenyl rings were refined as rigid groups. The remaining non-hydrogen atoms were refined anisotropically. Hydrogen atoms on the phenyl rings were included in calculated positions. Final fractional atomic coordinates and thermal parameters may be found in Table III.

Results and Discussion

Syntheses of Gold-Derivatized Clusters. The possibility exists for coordination of three $(R_3P)Au^+$ units on a $[Fe_3(CO)_9(\mu_3\text{-}P)]^{3-}$ frame if all of the potential hydrogen sites are replaced by gold. Both the silylphosphinidene cluster $(\mu\text{-H})_2Fe_3(CO)_9[\mu_3\text{-}PSi(i\text{-}Pr)_3]$ (**1**)[10] and the anionic cluster $[(\mu\text{-H})Fe_3(CO)_9(\mu_3\text{-}PH)]^-$ (**2**),[10] prepared by reaction of **1** with $[NBu_4]F$, are useful starting materials for the preparation of gold-derivatized clusters.

Reactions between the silylphosphinidene cluster **1** and 1 equiv of $(R_3P)AuCl$ occur over a period of 4 h to produce $(\mu\text{-H})_2Fe_3(CO)_9P[Au(PR_3)]$ (**3a**, R = Ph; **3b**, R = Et) with evolution of $(i\text{-Pr})_3SiCl$ (Scheme I). Replacement of the silyl group by $(R_3P)Au^+$ results in a shift of the CO stretching frequencies by 10 cm^{-1} to lower energy than in the parent cluster (see Table IV). The gold(I) fragment is assigned terminal coordination to the triply-bridging phosphorus atom (as opposed to a site on an Fe–P edge or an Fe_2P face) on the basis of the ^{31}P NMR spectrum, where the large $^2J_{PP}$ value of ~300 Hz between the PR_3 ligand and the cluster-bound phosphorus atom (P_c) is indicative of a *trans* arrangement of the two phosphorus nuclei.

Reactions between the desilylated cluster **2** and the gold halides are more facile than the reactions with **1**, and the same gold-capped clusters are produced in the time of mixing. Because **2** contains a hydrogen bound to the phosphorus atom while the products **3a,b** have the gold(I) fragment bound to the phosphorus atom, a low-temperature NMR experiment was performed in an attempt to observe an intermediate with the $(R_3P)Au^+$ fragment bridging an Fe–Fe edge of the cluster. When an NMR tube at 173 K containing $(Ph_3P)AuCl$ was treated with a 173 K CH_2Cl_2 solution of **2** and transferred to a precooled NMR probe, **3a** was the sole product observed. The fact the proton bound to the phosphorus atom in **2** migrates to the Fe–Fe edge after reaction with a $(R_3P)Au^+$ fragment indicates that the capping P atom is the thermodynamically preferred site of coordination for the gold-(I) fragment.

Reactions of $(Ph_3P)AuCl$ with the related phenylphosphinidene cluster $(\mu\text{-H})_2Fe_3(CO)_9(\mu_3\text{-PPh})$ as well as the isoelectronic sulfido cluster $(\mu\text{-H})_2Fe_3(CO)_9(\mu_3\text{-S})$ have been explored.[13] In $(\mu\text{-H})$-

Table II. Fractional Atomic Coordinates[a] and B_{iso}[b] Values (Å^2) for $(\mu\text{-H})Fe_3(CO)_9P[Au(PPh_3)]_2$ (**4a**)

	x	y	z	B_{iso}
Au(1)	0.26838(2)	0.04247(4)	0.10702(2)	4.19(2)
Au(2)	0.33375(2)	0.20392(3)	0.13794(2)	3.80(2)
Fe(1)	0.44801(9)	–0.00338(13)	0.15294(6)	4.31(9)
Fe(2)	0.46089(8)	0.16266(12)	0.13586(5)	3.89(8)
Fe(3)	0.46487(9)	0.04658(13)	0.07861(6)	4.21(8)
P_c	0.3798(2)	0.0707(2)	0.11353(10)	3.7(2)
P(1)	0.1656(2)	–0.0188(2)	0.10598(11)	4.2(2)
P(2)	0.2602(2)	0.2998(2)	0.16205(10)	4.0(2)
C(1)	0.4066(7)	0.0203(10)	0.1953(5)	5.9(8)
O(1)	0.3782(7)	0.0342(8)	0.2226(3)	8.8(7)
C(2)	0.4146(6)	–0.1087(9)	0.1465(4)	5.2(7)
O(2)	0.3900(5)	–0.1736(7)	0.1406(4)	7.6(6)
C(3)	0.5275(7)	–0.0221(10)	0.1758(4)	5.7(7)
O(3)	0.5788(6)	–0.0340(8)	0.1908(4)	8.1(6)
C(4)	0.4600(6)	0.2614(10)	0.1101(4)	4.9(7)
O(4)	0.4635(5)	0.3262(7)	0.0937(4)	7.7(7)
C(5)	0.4526(7)	0.2047(10)	0.1830(5)	5.8(7)
O(5)	0.4509(5)	0.2345(9)	0.2155(3)	8.4(7)
C(6)	0.5472(7)	0.1504(9)	0.1404(5)	5.8(8)
O(6)	0.6041(5)	0.1455(7)	0.1445(4)	7.5(7)
C(7)	0.4369(8)	–0.0437(10)	0.0501(5)	6.2(8)
O(7)	0.4168(7)	–0.1021(9)	0.0325(4)	10.1(8)
C(8)	0.4474(8)	0.1277(10)	0.0438(4)	5.6(7)
O(8)	0.4346(7)	0.1808(8)	0.0208(3)	8.9(8)
C(9)	0.5504(7)	0.0376(9)	0.0706(4)	5.5(7)
O(9)	0.6055(6)	0.0296(9)	0.0663(4)	9.2(8)
C(11)	0.0979(4)	0.0373(6)	0.0815(3)	4.2(6)
C(12)	0.0359(4)	0.0365(7)	0.0966(2)	6.4(8)
C(13)	–0.0173(3)	0.0737(8)	0.0753(3)	7.3(9)
C(14)	–0.0085(4)	0.1116(7)	0.0389(3)	7.0(9)
C(15)	0.0535(5)	0.1124(7)	0.0238(2)	7.5(9)
C(16)	0.1067(4)	0.0753(7)	0.0451(3)	6.3(8)
C(21)	0.1683(4)	–0.1231(5)	0.0819(3)	4.5(6)
C(22)	0.1137(4)	–0.1567(6)	0.0606(3)	5.8(7)
C(23)	0.1176(5)	–0.2373(6)	0.0424(3)	6.6(8)
C(24)	0.1760(6)	–0.2843(5)	0.0454(3)	8.4(11)
C(25)	0.2306(5)	–0.2507(6)	0.0667(4)	8.5(11)
C(26)	0.2267(4)	–0.1701(7)	0.0850(3)	6.2(8)
C(31)	0.1425(4)	–0.0409(6)	0.1551(2)	4.2(6)
C(32)	0.1059(4)	–0.1137(6)	0.1641(2)	5.7(7)
C(33)	0.0891(5)	–0.1279(6)	0.2026(3)	7.2(9)
C(34)	0.1088(5)	–0.0692(8)	0.2321(2)	7.5(10)
C(35)	0.1454(5)	0.0037(7)	0.2230(3)	7.5(10)
C(36)	0.1622(4)	0.0178(5)	0.1845(3)	6.2(8)
C(41)	0.2566(4)	0.2862(6)	0.2146(2)	4.3(6)
C(42)	0.2803(5)	0.2102(5)	0.2323(3)	5.7(7)
C(43)	0.2781(5)	0.1994(6)	0.2728(3)	6.7(9)
C(44)	0.2521(5)	0.2646(7)	0.2955(2)	6.7(9)
C(45)	0.2283(5)	0.3407(6)	0.2778(2)	6.2(8)
C(46)	0.2306(4)	0.3515(5)	0.2373(3)	5.1(7)
C(51)	0.2850(4)	0.4110(4)	0.1551(2)	3.7(5)
C(52)	0.3515(4)	0.4311(5)	0.1609(2)	4.8(6)
C(53)	0.3724(3)	0.5168(6)	0.1579(3)	5.4(7)
C(54)	0.3268(5)	0.5823(4)	0.1491(3)	6.6(9)
C(55)	0.2604(4)	0.5622(5)	0.1433(3)	6.0(8)
C(56)	0.2395(3)	0.4765(6)	0.1463(3)	5.3(7)
C(61)	0.1770(3)	0.2909(6)	0.1417(3)	4.8(6)
C(62)	0.1265(4)	0.2634(6)	0.1645(2)	5.4(7)
C(63)	0.0629(4)	0.2552(7)	0.1478(3)	7.0(10)
C(64)	0.0498(3)	0.2745(7)	0.1082(3)	6.4(9)
C(65)	0.1003(5)	0.3020(7)	0.0853(2)	7.7(10)
C(66)	0.1639(4)	0.3102(7)	0.1021(3)	6.3(9)

[a] Estimated standard deviations in the least significant digit(s) are given in parentheses. [b] B_{iso} is the mean of the principal axes of the thermal ellipsoid.

Table III. Fractional Atomic Coordinates[a] and B_{iso}[b] Values (Å^2) for $Fe_3(CO)_9P[Au(PPh_3)]_3$ (**5a**)

	x	y	z	B_{iso}		x	y	z	B_{iso}
Au(1)	0.69729(9)	0.64395(6)	0.35834(7)	2.81(6)	C(142)	0.944(2)	0.563(1)	0.461(9)	4.0(4)
Au(2)	0.63061(8)	0.67254(6)	0.20122(7)	2.51(5)	C(143)	0.986(3)	0.505(2)	0.450(2)	4.0(4)
Au(3)	0.55627(9)	0.75105(6)	0.32313(7)	2.65(5)	C(144)	0.987(3)	0.478(1)	0.384(3)	4.0(4)
Fe(1)	0.4491(3)	0.6564(2)	0.3576(3)	3.4(2)	C(145)	0.946(3)	0.510(2)	0.329(2)	4.0(4)
Fe(2)	0.4711(3)	0.6740(2)	0.2257(2)	2.7(2)	C(146)	0.904(2)	0.569(2)	0.3397(6)	4.0(4)
Fe(3)	0.4772(3)	0.5537(2)	0.2788(3)	3.1(2)	C(151)	0.79984	0.63662	0.51457	3.8(4)
P_c	0.5682(6)	0.6301(4)	0.3037(4)	2.6(4)	C(152)	0.739(2)	0.589(1)	0.521(1)	3.8(4)
P(1)	0.8162(6)	0.6520(4)	0.4281(5)	3.3(4)	C(153)	0.706(3)	0.578(2)	0.585(2)	3.8(4)
P(3)	0.5957(6)	0.8521(4)	0.3611(5)	2.6(4)	C(154)	0.734(3)	0.616(3)	0.642(1)	3.8(4)
P(2)	0.7248(6)	0.6828(4)	0.1176(5)	2.7(4)	C(155)	0.794(3)	0.664(2)	0.635(1)	3.8(4)
C(1)	0.406(2)	0.733(2)	0.381(2)	3.3(16)	C(156)	0.827(2)	0.674(1)	0.571(1)	3.8(4)
O(1)	0.374(2)	0.779(1)	0.402(1)	5.5(14)	C(211)	0.697(1)	0.630(1)	0.046(1)	2.9(7)
C(2)	0.501(3)	0.638(2)	0.437(2)	5.4(22)	C(212)	0.722(1)	0.646(1)	−0.019(1)	3.2(7)
O(2)	0.532(2)	0.629(2)	0.490(2)	6.8(19)	C(213)	0.698(2)	0.605(1)	−0.075(1)	3.8(8)
C(3)	0.366(3)	0.613(2)	0.370(2)	5.8(25)	C(214)	0.651(2)	0.549(1)	−0.065(1)	3.9(8)
O(3)	0.306(2)	0.579(2)	0.383(2)	8.0(19)	C(215)	0.626(1)	0.534(1)	0.000(1)	3.1(7)
C(4)	0.454(2)	0.628(2)	0.146(2)	3.1(16)	C(216)	0.650(1)	0.574(1)	0.056(1)	3.5(7)
O(4)	0.440(2)	0.602(1)	0.097(1)	4.2(13)	C(221)	0.731(1)	0.765(1)	0.084(1)	2.7(7)
C(5)	0.480(2)	0.752(2)	0.188(2)	2.7(14)	C(222)	0.807(1)	0.792(1)	0.067(1)	2.9(7)
O(5)	0.478(2)	0.805(1)	0.159(1)	3.8(12)	C(223)	0.810(1)	0.855(1)	0.040(1)	2.9(7)
C(6)	0.364(2)	0.682(2)	0.246(2)	2.9(15)	C(224)	0.738(1)	0.892(1)	0.030(1)	4.1(8)
O(6)	0.296(2)	0.685(1)	0.245(1)	4.7(14)	C(225)	0.662(1)	0.866(1)	0.048(1)	4.1(8)
C(7)	0.502(3)	0.500(2)	0.347(2)	5.2(22)	C(226)	0.659(1)	0.802(1)	0.074(1)	2.9(7)
O(7)	0.527(2)	0.466(1)	0.393(2)	6.6(17)	C(231)	0.828(1)	0.660(1)	0.145(1)	3.2(7)
C(8)	0.529(2)	0.510(2)	0.214(2)	3.0(16)	C(232)	0.880(2)	0.624(1)	0.104(1)	3.9(8)
O(8)	0.552(2)	0.481(1)	0.171(1)	4.4(12)	C(233)	0.961(2)	0.611(1)	0.128(1)	5.2(9)
C(9)	0.374(2)	0.528(2)	0.249(2)	3.2(16)	C(234)	0.991(1)	0.633(1)	0.192(2)	5.5(10)
O(9)	0.308(2)	0.511(1)	0.236(1)	4.5(12)	C(235)	0.939(2)	0.669(2)	0.233(1)	7.6(13)
C(111)	0.800(3)	0.637(2)	0.515(2)	3.8(4)	C(236)	0.858(2)	0.682(1)	0.210(1)	6.7(12)
C(112)	0.811(3)	0.573(2)	0.542(2)	3.8(4)	C(311)	0.664(1)	0.898(1)	0.308(1)	2.9(7)
C(113)	0.792(3)	0.561(1)	0.609(2)	3.8(4)	C(312)	0.705(1)	0.863(1)	0.259(1)	2.1(6)
C(114)	0.763(3)	0.611(2)	0.650(2)	3.8(4)	C(313)	0.763(1)	0.894(1)	0.220(1)	1.9(6)
C(115)	0.752(3)	0.674(2)	0.622(2)	3.8(4)	C(314)	0.780(1)	0.961(1)	0.230(1)	3.6(7)
C(116)	0.770(3)	0.687(1)	0.555(2)	3.8(4)	C(315)	0.739(2)	0.996(1)	0.279(1)	3.1(7)
C(121)	0.868(1)	0.730(8)	0.427(1)	1.9(6)	C(316)	0.681(1)	0.965(1)	0.318(1)	4.5(9)
C(122)	0.842(1)	0.780(1)	0.381(1)	3.9(8)	C(321)	0.642(1)	0.850(1)	0.447(1)	3.3(7)
C(123)	0.885(2)	0.839(9)	0.381(1)	3.4(7)	C(322)	0.708(1)	0.888(1)	0.472(1)	3.4(7)
C(124)	0.954(2)	0.848(1)	0.426(1)	4.5(9)	C(323)	0.736(1)	0.884(1)	0.541(1)	4.7(9)
C(125)	0.980(1)	0.798(1)	0.471(1)	6.6(12)	C(324)	0.697(2)	0.841(1)	0.585(1)	5.7(10)
C(126)	0.937(2)	0.739(1)	0.471(1)	5.6(10)	C(325)	0.631(2)	0.802(1)	0.560(1)	6.5(11)
C(131)	0.902(2)	0.595(2)	0.406(2)	4.0(4)	C(326)	0.603(1)	0.807(1)	0.491(1)	4.2(8)
C(132)	0.878(2)	0.535(2)	0.376(2)	4.0(4)	C(331)	0.508(1)	0.907(1)	0.365(1)	2.4(6)
C(133)	0.936(3)	0.491(2)	0.356(2)	4.0(4)	C(332)	0.480(1)	0.934(1)	0.425(1)	3.3(7)
C(134)	1.020(2)	0.506(2)	0.365(2)	4.0(4)	C(333)	0.408(1)	0.972(1)	0.422(1)	4.3(8)
C(135)	1.045(2)	0.566(2)	0.394(2)	4.0(4)	C(334)	0.364(1)	0.983(1)	0.360(1)	2.8(7)
C(136)	0.986(3)	0.610(2)	0.415(2)	4.0(4)	C(335)	0.392(1)	0.956(1)	0.300(1)	2.7(6)
C(141)	0.90247	0.59523	0.40561	4.0(4)	C(336)	0.464(1)	0.917(1)	0.303(1)	2.0(6)

[a] Estimated standard deviations in the least significant digit(s) are given in parentheses. [b] B_{iso} is the mean of the principal axes of the thermal ellipsoid.

$[\mu$-$Au(PPh_3)]Fe_3(CO)_9(\mu_3$-PPh), the first $(Ph_3P)Au^+$ fragment interacts with an Fe–Fe edge of the cluster and is characterized by a correspondingly small $^2J_{PP}$ of 38 Hz.[13a] The second gold fragment in $[Au(PPh_3)]_2Fe_3(CO)_9(\mu_3$-PPh) interacts with the Fe_3 face of the cluster, opposite of the phosphinidene ligand, and forms a Au···Au bond to the first fragment. No direct interaction with phosphorus is observed in either of these clusters because of the presence of the phenyl capping group. Surprisingly, the Au_2 derivative of the sulfido-capped analogue, $[Au(PPh_3)]_2Fe_3(CO)_9(\mu_3$-S),[13b] is isostructural with the phenylphosphinidene analogue, even though there is no capping substituent blocking coordination to sulfur. Thus, the fact that the primary site of interaction between a $(R_3P)Au^+$ fragment and the $[H_2Fe_3(CO)_9P]^-$ cluster is the terminal site on the phosphorus heteroatom is a noteworthy feature of **3a,b**.

The Au_2 clusters $(\mu$-$H)Fe_3(CO)_9P[Au(PR_3)]_2$ (**4a**, R = Ph; **4b**, R = Et) are accessible by reaction of the appropriate number of equivalents of $(R_3P)AuCl$ with the starting clusters, **1** or **2** (Scheme I). The chemical shift and multiplicity of the $^{31}P\{^1H\}$ NMR resonance for P_c are indicative of the number of $(R_3P)Au^+$ units bound to the cluster. For instance, the doublet at δ 390.3 ppm ($^2J_{PP}$ = 314 Hz) for **3a** is replaced by a triplet at δ 252.3 ppm ($^2J_{PP}$ = 192 Hz) for the digold cluster, **4a**, indicating coupling to two equivalent PPh_3 ligands. As expected, a single doublet is observed for the PPh_3 ligands bound to gold. An attempt was made to prepare the asymmetric Au_2 cluster with two different phosphine ligands bound to the gold cations. Although several routes were attempted to this complex, the most straightforward proved to be an exchange reaction between the two symmetric Au_2 clusters (eq 1). After stirring of a 1:1 mixture of **4a,b** at

$$\underset{\textbf{4a}}{(\mu\text{-H})Fe_3(CO)_9P[Au(PPh_3)]_2} + \underset{\textbf{4b}}{(\mu\text{-H})Fe_3(CO)_9P[Au(PEt_3)]_2} \rightleftharpoons 2\underset{\textbf{4c}}{(\mu\text{-H})Fe_3(CO)_9P\{[Au(PPh_3)][Au(PEt_3)]\}} \quad (1)$$

room temperature for 4 h, NMR analysis of the solution shows the asymmetric cluster, **4c**, and the symmetric clusters, **4a,b**, in an approximate 2:1:1 **4c**:**4a**:**4b** statistical ratio. The P_c resonance in the ^{31}P NMR spectrum for **4c** is an overlapping doublet of doublets at δ 260.7 ppm, intermediate in chemical shift between **4a** and **4b**. It is not clear whether this reaction proceeds by interchange of phosphine ligands or $(R_3P)Au^+$ fragments between **4a** and **4b**, although $(R_3P)M^+$ interchange reactions between homometallic Au_2, Cu_2, and Ag_2 clusters have been utilized to prepare mixed-metal clusters.[9e]

Table IV. Infrared CO Stretching Frequencies,[a] $^{31}P\{^1H\}$ NMR Data,[b] and ^1H NMR Data[b] for Au-Substituted Clusters

		$^{31}P\{^1H\}$ NMR			^1H NMR				
compound	IR, cm^{-1} ν(CO)	$\delta(\mu_3\text{-P})$	$\delta(PR_3)$	$^2J_{PP}$	assgnt	δ	$^2J_{HP}$	$^3J_{HP}$	$^3J_{HH}$
$(\mu\text{-H})_2Fe_3(CO)_9P[Au(PPh_3)]$ (**3a**)	2079 w, 2044 s, 2018 vs, 1990 m, 1972 w[c]	390.3, d	40.8, d	314[d]	μ-H	−23.53, d	20.1		
					C_6H_5	7.47, 7.25, m[h]			
$(\mu\text{-H})Fe_3(CO)_9P[Au(PPh_3)]_2$ (**4a**)	2050 m, 2016 vs, 1984 vs, 1976 sh[d]	252.3, t	45.3, d	192[e]	μ-H	−22.80, d	31.1		
					C_6H_5	7.3, m[g]			
$Fe_3(CO)_9P[Au(PPh_3)]_3$ (**5a**)	2021 vs, 1969 vs, 1960 vs, 1943 sh, 1921 w br[e]	125.7, q	45.1, d	147[g]	C_6H_5	7.36, 7.10, m[g]			
$(\mu\text{-H})_2Fe_3(CO)_9P[Au(PEt_3)]$ (**3b**)	2079 w, 2044 s, 2016 vs, 1988 m, 1971 w[c]	405.8, d	42.8, d	313[e]	μ-H	−23.86, d	21.0		
					CH_2	2.05, dqd	9.7	7.7	3.1 ($^4J_{HP}$)
					CH_3	1.33, dt		18.9	7.7[g]
$(\mu\text{-H})Fe_3(CO)_9P[Au(PEt_3)]_2$ (**4b**)	2043 m, 2013 vs, 1980 vs, 1971 sh[f]	264.1, t	47.6, d	192[e]	μ-H	−22.83, d	29.5		
					CH_2	2.00, dq	7.2		7.7
					CH_3	1.30, dt		18.7	7.7[g]
$Fe_3(CO)_9P[Au(PEt_3)]_3$ (**5b**)	2019 vs, 1964 vs, 1955 vs, 1938 sh, 1914 w br[e]	149.6, q	50.0, d	146[e]	CH_2	1.90, dq	7.5		7.7
					CH_3	1.26, dt		18.5	7.7[g]
$(\mu\text{-H})Fe_3(CO)_9P\{[Au(PEt_3)]\text{-}[Au(PPh_3)]\}$ (**4c**)		260.7, dd	47.3, d (PEt_3)	198					
			45.7, d (PPh_3)	192[g]					

[a] Abbreviations: vs = very strong, s = strong, m = medium, w = weak, vw = very weak, sh = shoulder. [b] δ reported in ppm, J reported in Hz. Abbreviations: s = singlet, d = doublet, m = multiplet, t = triplet, q = quartet. [c] Hexanes. [d] Benzene, [e] Dichloromethane. [f] Toluene. [g] Dichloromethane-d_2. [h] Benzene-d_6.

Scheme I

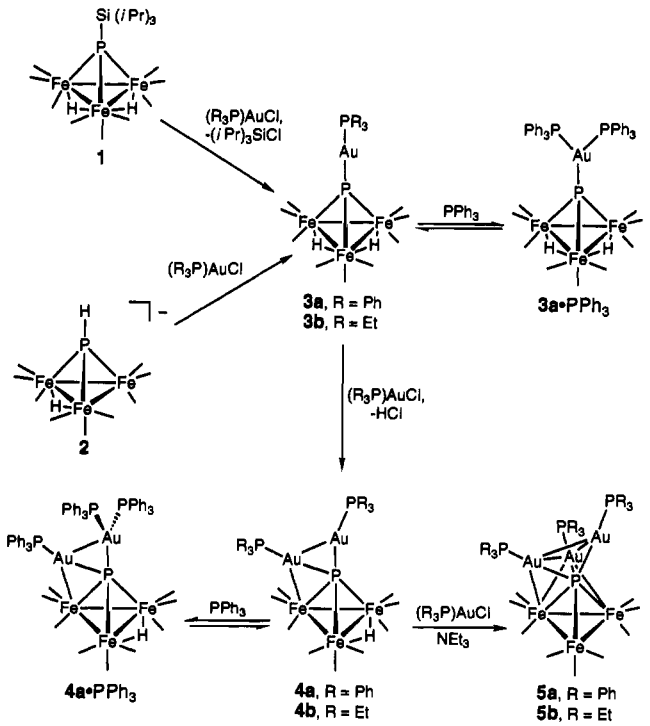

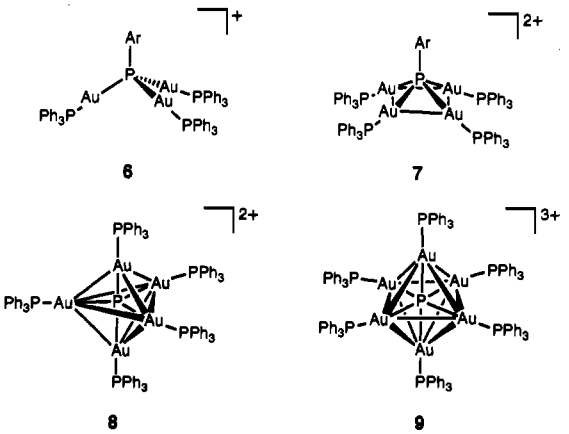

Like the Au_2 clusters, the Au_3 clusters $Fe_3(CO)_9P[Au(PR_3)]_3$ (**5a**, R = Ph; **5b**, R = Et) can be prepared from reactions of **1** or **2** with 3 equiv of the gold reagent (Scheme I). The third substitution is the slowest, and it is necessary to add NEt_3 to accelerate the reaction rate. In the trigold cluster, **5a**, the ^{31}P resonance for P_c is a quartet at δ 125.7 ppm ($^2J_{PP}$ = 147 Hz), with a corresponding doublet for the phosphine ligands at δ 45.1 ppm. The successive substitution of additional gold units is characterized by a marked upfield shift of the ^{31}P resonance for P_c together with a decrease in the $^2J_{PP}$ value that reflects the change in the average environment of the gold-bound phosphine ligands with respect to P_c. Spectroscopic data for the gold-substituted clusters are summarized in Table IV.

^{31}P NMR data for the structurally-related aurated phosphorus cations and dications $[(o\text{-tolyl})P\{Au(PPh_3)\}_3]^+$ (**6**), $[(o\text{-tolyl})P\{Au(PPh_3)\}_4]^{2+}$ (**7**),[15] and the phosphorus-centered clusters $[P\{Au(PPh_3)\}_5]^{2+}$ (**8**)[6a] and $[P\{Au(PPh_3)\}_6]^{3+}$ (**9**)[6b] are collected in Table V. The $^2J_{PP}$ values for **6**–**9** are comparable to those observed for the gold-substituted clusters, **3**–**5**. In agreement with the general trends observed for **3**–**5**, the addition of a $(Ph_3P)Au^+$ fragment to **6** producing **7** results in a decrease in the $^2J_{PP}$ value from 249 to 196 Hz and an upfield shift in the ^{31}P resonance by ~35 ppm. The upfield chemical shift observed for the central P atom of 288 ppm upon addition of a $(Ph_3P)Au^+$ fragment to **8** producing **9** is quite large, while the change in coupling from 186 to 167 Hz is less dramatic. For the aurated cations, **6**–**9**, it is necessary to perform a low-temperature NMR experiment to observe P_c–PR_3 coupling,[6,15] presumably because of rapid intermolecular exchange of $(Ph_3P)Au^+$ units. Such intermolecular exchange reactions are not rapid at room temperature for the gold-substituted Fe_3P clusters.

X-ray Structure Determinations. The structures of the Au_2 cluster, **4a**, and the Au_3 cluster, **5a**, were determined by single-crystal X-ray diffraction to ascertain the coordination modes of the gold fragments. The structure of **4a** (Figure 1) consists of a $[HFe_3(CO)_9(\mu_3\text{-P})]^{2-}$ cluster frame coordinated to a Au···Au-bonded $[Au_2(PPh_3)_2]^{2+}$ unit. Distinct coordination environments are observed for each $(Ph_3P)Au^+$ fragment. The first $(Ph_3P)Au^+$ unit is bound to the cluster exclusively through the Fe_3P phosphorus atom (P_c), in a position analogous to that presumably adopted by the Au_1 derivatives. The Au–PPh_3 vector is tilted by 16° with respect to the normal of the Fe_3 plane to accommodate bonding to the second gold fragment (see Figure 2a). This apically-coordinated Au(I) ion is bound at very similar distances

(15) Schmidbaur, H.; Zeller, E.; Weidenhiller, G.; Steigelmann, O.; Beruda, H. *Inorg. Chem.* **1992**, *31*, 2370.

Table V. Spectroscopic and Structural Data for Aurated Phosphorus Cations

	$\delta(P_c)$, ppm	$\delta(PR_3)$, ppm	$^2J(P,P)$, Hz	Au–P_c(av), Å	Au–PR_3(av) Å	Au···Au(av), Å
$[(o\text{-tolyl})P\{Au(PPh_3)\}_3]^+$ (**6**)[a]	−19 (quart)	45 (d)	249	2.31(2)	2.29(2)	3.68(4)
$[(o\text{-tolyl})P\{Au(PPh_3)\}_4]^{2+}$ (**7**)[a]	−56 (quint)	38 (d)	196	2.37(1)	2.293(7)	2.97(5)
$[P\{Au(PPh_3)\}_5]^{2+}$ (**8**)[b]	122 (sext)	40 (d)	186			
$[P\{Au(PPh_3)\}_6]^{3+}$ (**9**)[c]	−166 (sept)	37 (d)	167			

[a] From ref 15. [b] From ref 6a. [c] From ref 6b.

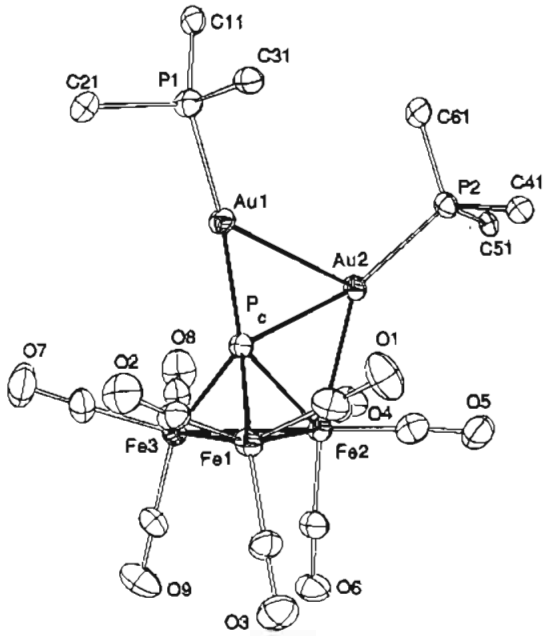

Figure 1. ORTEP plot for $HFe_3(CO)_9P[Au(PPh_3)]_2$ (**4a**) with thermal ellipsoids at the 50% probability level. Only the ipso carbon atoms of the phenyl rings are included for clarity.

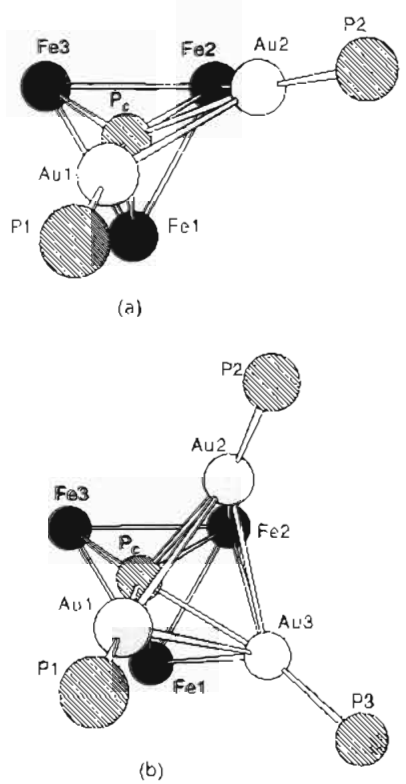

Figure 2. (a) Top view of the $Fe_3P[Au_2P_2]$ core in **4a**. (b) Top view of the $Fe_3P[Au_3P_3]$ core in **5a**.

to P_c and the phosphorus atom of the triphenylphosphine ligand (Au(1)–P_c = 2.316(3) Å; Au(1)–P(1) = 2.301(3) Å). The second $(Ph_3P)Au^+$ unit is connected to the first by a Au···Au bond of typical length (2.991(1) Å)[16] and also interacts with the Fe(2)-P_c edge of the cluster; the Au(2)–P_c distance of 2.428(3) Å is more than 0.1 Å longer than the bond from P_c to Au(1). As a result of coordinating the Au_2 fragment to the Fe(2)–P(1) edge of the cluster, P_c is bound at shorter distances to Fe(1) and Fe(3) than to Fe(2) (Fe(2)–P_c = 2.278(4) Å; Fe(3)–P_c = 2.194(4) Å; Fe(1)–P_c = 2.200(4) Å). The position of the hydride ligand in **4a** was not located in the X-ray diffraction experiment; however, the Fe(1)–Fe(3) distance (2.693(3) Å) is ca. 0.04 Å longer than the two other Fe–Fe distances (Fe(1)–Fe(2) = 2.645(3) Å; Fe(2)–Fe(3) = 2.656(3) Å), suggesting that the hydride ligand is located along the Fe(1)–Fe(3) edge. Selected bond lengths and angles for **4a** are displayed in Table VI.

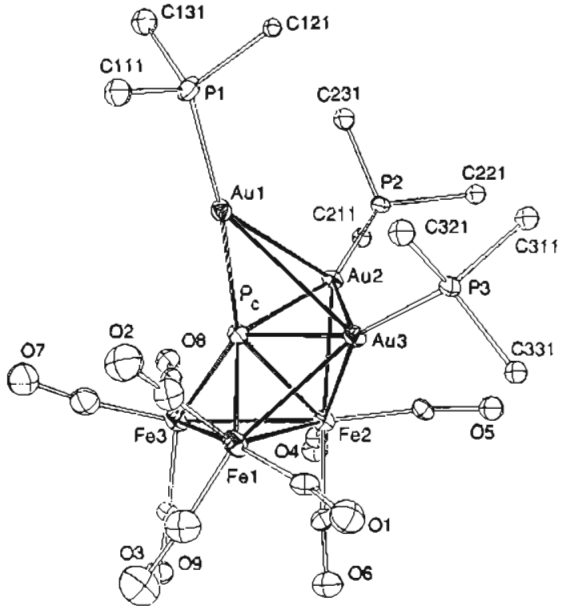

Figure 3. ORTEP plot for $Fe_3(CO)_9P[Au(PPh_3)]_3$ (**5a**) with thermal ellipsoids at the 50% probability level. Only the ipso carbon atoms of the phenyl rings are included for clarity.

The structure of **5a** (Figure 3) consists of a $[Fe_3(CO)_9(\mu_3\text{-}P)]^{3-}$ cluster frame coordinated to a Au···Au-bonded triangular $[Au_3(PPh_3)_3]^{3+}$ unit. The relationship between the structure of **4a** and **5a** can be easily seen in Figure 2b, where Au(1) and Au(2) adopt similar positions in both structures. The additional $(Ph_3P)Au^+$ fragment in **5a** interacts with both Au(1) and Au(2) as well as the P_c–Fe(1)–Fe(2) face of the cluster. The three Au···Au distances in **5a** (Au–Au(av) = 3.2 Å) are elongated by ~0.2 Å over the distance observed for the single Au···Au interaction in **4a**. The bond distances describing the interaction of Au(1) and Au(2) with P_c in **5a** do not differ significantly from those for **4a**, although the orientation of the Au(1)–Au(2) edge with respect to the Fe(1)–P(1) bond is significantly different as a result of the interaction with Au(3) in **5a** (Figure 2b). The third $(Ph_3P)Au^+$ unit is bound at the longest distance to P_c of the three gold ions (Au(3)–P_c = 2.502(8) Å). The Au–Fe bond distances range from 2.675(5) to 2.772(5) Å. Surprisingly, the interaction of Au(3) does not significantly affect the Fe(1)–Fe(2) distance, and the Fe_3 unit can be described as a nearly equilateral triangle (Fe–Fe = 2.645(7)–2.659(7) Å). The Au_3 plane makes

(16) Pathaneni, S. S.; Desiraju, G. R. *J. Chem. Soc., Dalton Trans.* **1993**, 319.

Table VI. Selected Bond Lengths (Å) and Angles (deg) for $(\mu\text{-H})Fe_3(CO)_9P[Au(PPh_3)]_2$ (**4a**)[a]

Au–Au	Au(1)–Au(2)	2.991(1)				
Au–Fe	Au(2)–Fe(2)	2.678(2)				
Fe–Fe	Fe(1)–Fe(2)	2.645(3)	Fe(1)–Fe(3)	2.693(3)	Fe(2)–Fe(3)	2.656(3)
Fe–P	Fe(1)–P_c	2.200(4)	Fe(2)–P_c	2.278(4)	Fe(3)–P_c	2.194(4)
Au–P_c	Au(1)–P_c	2.316(3)	Au(2)–P_c	2.428(3)		
Au–P	Au(1)–P(1)	2.301(3)	Au(2)–P(2)	2.295(3)		
Fe–CO	Fe(1)–C(1)	1.76(1)	Fe(2)–C(4)	1.76(1)	Fe(3)–C(7)	1.78(2)
	Fe(1)–C(2)	1.77(2)	Fe(2)–C(5)	1.75(2)	Fe(3)–C(8)	1.75(1)
	Fe(1)–C(3)	1.78(1)	Fe(2)–C(6)	1.77(1)	Fe(3)–C(9)	1.79(1)
C–O	C(1)–O(1)	1.14(2)	C(4)–O(4)	1.15(2)	C(7)–O(7)	1.15(2)
	C(2)–O(2)	1.13(2)	C(5)–O(5)	1.20(2)	C(8)–O(8)	1.16(2)
	C(3)–O(3)	1.16(2)	C(6)–O(6)	1.16(2)	C(9)–O(9)	1.15(2)
Fe–Fe–Fe	Fe(1)–Fe(2)–Fe(3)	61.06(7)	Fe(2)–Fe(3)–Fe(1)	59.26(7)	Fe(2)–Fe(1)–Fe(3)	59.68(7)
Au–Au–Fe	Au(1)–Au(2)–Fe(2)	101.91(5)				
Au–Fe–Fe	Au(2)–Fe(2)–Fe(1)	96.65(7)	Au(2)–Fe(2)–Fe(3)	104.50(8)		
Fe–P–Fe	Fe(2)–P_c–Fe(1)	72.4(1)	Fe(2)–P_c–Fe(3)	72.8(1)	Fe(1)–P_c–Fe(3)	75.6(1)
Fe–Fe–C	Fe(1)–Fe(2)–C(4)	162.1(5)	Fe(2)–Fe(3)–C(7)	155.6(5)	Fe(3)–Fe(2)–C(4)	102.5(5)
	Fe(1)–Fe(2)–C(5)	98.1(5)	Fe(2)–Fe(3)–C(8)	90.2(5)	Fe(3)–Fe(2)–C(5)	159.1(5)
	Fe(1)–Fe(2)–C(6)	89.3(5)	Fe(2)–Fe(3)–C(9)	103.7(5)	Fe(3)–Fe(2)–C(6)	85.4(5)
	Fe(1)–Fe(3)–C(7)	103.7(5)	Fe(2)–Fe(1)–C(1)	92.2(5)	Fe(3)–Fe(1)–C(1)	144.2(5)
	Fe(1)–Fe(3)–C(8)	144.4(5)	Fe(2)–Fe(1)–C(2)	154.7(5)	Fe(3)–Fe(1)–C(2)	102.4(5)
	Fe(1)–Fe(3)–C(9)	107.5(5)	Fe(2)–Fe(1)–C(3)	98.8(5)	Fe(3)–Fe(1)–C(3)	107.2(5)
P–Au–P	P_c–Au(1)–P(1)	165.90(12)	P_c–Au(2)–P(2)	160.67(12)		
Au–P–Au	Au(1)–P_c–Au(2)	78.12(10)				
Fe–Fe–P	Fe(1)–Fe(2)–P_c	52.5(1)	Fe(2)–Fe(1)–P_c	55.2(1)	Fe(3)–Fe(2)–P_c	52.1(1)
	Fe(1)–Fe(3)–P_c	52.3(1)	Fe(2)–Fe(3)–P_c	55.1(1)	Fe(3)–Fe(1)–P_c	52.1(1)
Au–Au–P	Au(1)–Au(2)–P_c	49.26(8)	Au(2)–Au(1)–P_c	52.61(8)		
	Au(1)–Au(2)–P(2)	112.07(9)	Au(2)–Au(1)–P(1)	137.4(1)		
Au–P–Fe	Au(1)–P_c–Fe(1)	123.0(2)	Au(1)–P_c–Fe(2)	147.2(2)	Au(1)–P_c–Fe(3)	136.1(2)
	Au(2)–P_c–Fe(1)	118.3(2)	Au(2)–P_c–Fe(2)	69.3(1)	Au(2)–P_c–Fe(3)	131.7(2)
Fe–Au–P	Fe(2)–Au(2)–P_c	52.72(8)	Fe(2)–Au(2)–P(2)	144.9(1)		
Au–Fe–P	Au(2)–Fe(2)–P_c	58.00(9)				
Fe–P–Fe	Fe(1)–P_c–Fe(3)	75.6(1)	Fe(2)–P_c–Fe(3)	72.8(1)	Fe(2)–P_c–Fe(1)	72.4(1)
Au–Fe–C	Au(2)–Fe(2)–C(4)	79.9(4)	Au(2)–Fe(2)–C(5)	75.1(5)	Au(2)–Fe(2)–C(6)	170.0(5)
P–Fe–C	P_c–Fe(1)–C(1)	100.1(5)	P_c–Fe(2)–C(5)	115.6(5)	P_c–Fe(3)–C(7)	101.0(5)
	P_c–Fe(1)–C(2)	94.5(5)	P_c–Fe(2)–C(4)	112.7(5)	P_c–Fe(3)–C(8)	96.3(5)
	P_c–Fe(1)–C(3)	151.6(5)	P_c–Fe(2)–C(6)	131.6(5)	P_c–Fe(3)–C(9)	155.0(5)
C–Fe–C	C(1)–Fe(1)–C(2)	95.4(7)	C(4)–Fe(2)–C(5)	98.0(7)	C(7)–Fe(3)–C(8)	98.3(7)
	C(1)–Fe(1)–C(3)	103.9(7)	C(5)–Fe(2)–C(6)	96.1(7)	C(8)–Fe(3)–C(9)	96.6(7)
	C(2)–Fe(1)–C(3)	98.2(7)	C(4)–Fe(2)–C(6)	96.8(6)	C(7)–Fe(3)–C(9)	98.1(7)
Fe–C–O	Fe(1)–C(1)–O(1)	175(1)	Fe(2)–C(4)–O(4)	176(1)	Fe(3)–C(7)–O(7)	178(2)
	Fe(1)–C(2)–O(2)	178(2)	Fe(2)–C(5)–O(5)	176(1)	Fe(3)–C(8)–O(8)	179(2)
	Fe(1)–C(3)–O(3)	180(1)	Fe(2)–C(6)–O(6)	177(1)	Fe(3)–C(9)–O(9)	178(1)
Au–P–C	Au(1)–P(1)–C(11)	110.5(3)	Au(1)–P(1)–C(21)	108.7(3)	Au(1)–P(1)–C(31)	119.1(3)
	Au(2)–P(2)–C(41)	111.7(3)	Au(2)–P(2)–C(51)	110.2(3)	Au(2)–P(2)–C(61)	115.7(3)

[a] Estimated standard deviations in the least significant digit(s) are given in parentheses.

a dihedral angle of 46° with respect to the Fe_3 plane. P_c is once again displaced from the center of the Fe_3 triangle, and it is bound ~0.13 Å more strongly to Fe(3) (Fe(3)–P_c = 2.18(1) Å), which does not interact with the Au_3 triangle, than Fe(1) or Fe(2) (Fe(1)–P_c = 2.31(1) Å; Fe(2)–P(1) = 2.32(1) Å). Selected bond lengths and angles for **5a** are displayed in Table VII.

The metric parameters for the structurally related Au_3 cation **6** and Au_4 dication **7** are collected in Table V.[15] In **6**, the Au–P_c and Au–PPh_3 distances average 2.31(2) and 2.29(2) Å, respectively, very similar in magnitude to the parameters involving Au(1) in **4a**. No Au···Au bonding (Au···Au = 3.7 Å) is observed in the Au_3 cation **6**. When an additional gold fragment is added to **6**, a square pyramidal structure containing a square array of golds is observed (Au···Au(av) = 2.97 Å). The Au–PPh_3 distances do not change, but the Au–P_c distances increase by 0.06 Å. For the case of the gold-substituted transition metal clusters, the Au–P_c distances seem to be determined by optimization of bonding to both the Fe_3 framework and P_c rather than being simply related to the coordination number of the phosphorus atom.

A similar series of gold-substituted clusters is obtained from sequential replacement of the cluster-bound hydrogen atoms in the butterfly borane cluster $HFe_4(CO)_{12}BH_2$ (**10**) with $(R_3P)Au^+$ fragments.[17] The initial $(R_3P)Au^+$ fragment replaces a hydrogen bound to a B–Fe_w bond.[17a] Analogously to **4a**, the second gold(I) fragment adds with formation of a Au···Au bond to the first.[17b] Two different isomers are observed for the Au_2 clusters, depending

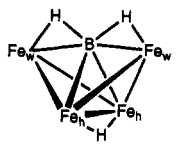

10

on the bulk of the phosphine ligand bound to gold.[17c] For small phosphines, the second gold fragment interacts with the second B–Fe_w bond, while, for large phosphines, the second gold fragment interacts with a B–Fe_h bond. A third gold fragment can also be added to produce an encapsulated boride cluster, $Fe_4(CO)_{12}B[Au(PPh_3)]_3$.[17d] The coordination environment about boron in the Au_3 cluster is quite similar to that observed for **5a**; however, only two Au···Au bonding interactions are observed: one between the two gold fragments bound to Fe_w–B edges and

(17) (a) Housecroft, C. E.; Rheingold, A. L. *J. Am. Chem. Soc.* **1986**, *108*, 6420. (b) Housecroft, C. E.; Rheingold, A. L. *Organometallics* **1987**, *6*, 1332. (c) Housecroft, C. E.; Shongwe, M. S.; Rheingold, A. L. *Organometallics* **1989**, *8*, 2651. (d) Harpp, K. S.; Housecraft, C. E.; Rheingold, A. L.; Shongwe, M. S. *J. Chem. Soc., Chem. Commun.* **1988**, 965. (e) Harpp, K. S.; Housecroft, C. E. *J. Organomet. Chem.* **1988**, *340*, 389. (f) Shipperfield, A. K.; Housecroft, C. E.; Rheingold, A. L. *Organometallics* **1990**, *9*, 681. (g) Housecroft, C. E.; Shonge, M. S.; Rheingold, A. L.; Zanello, P. *J. Organomet. Chem.* **1991**, *408*, 7. (h) Draper, S. M.; Housecroft, C. E.; Rees, J. E.; Shongwe, M. S.; Haggerty, B. E.; Rheingold, A. L. *Organometallics* **1992**, *11*, 2356.

Table VII. Selected Bond Lengths (Å) and Angles (deg) for $Fe_3(CO)_9P[Au(PPh_3)]_3$ (**5a**)[a]

Au–Au	Au(1)–Au(2)	3.245(2)	Au(1)–Au(3)	3.209(2)	Au(2)–Au(3)	3.167(2)
Au–Fe	Au(2)–Fe(2)	2.665(5)	Au(3)–Fe(1)	2.711(5)	Au(3)–Fe(2)	2.772(5)
Fe–Fe	Fe(1)–Fe(2)	2.645(7)	Fe(1)–Fe(3)	2.652(7)	Fe(2)–Fe(3)	2.659(7)
Fe–P	Fe(1)–P_c	2.32(1)	Fe(2)–P_c	2.31(1)	Fe(3)–P_c	2.18(1)
Au–P_c	Au(1)–P_c	2.314(9)	Au(2)–P_c	2.455(9)	Au(3)–P_c	2.502(8)
Au–P	Au(1)–P(1)	2.303(10)	Au(2)–P(2)	2.314(9)	Au(3)–P(3)	2.267(8)
Fe–CO	Fe(1)–C(1)	1.77(3)	Fe(2)C(4)	1.83(3)	Fe(3)–C(7)	1.75(4)
	Fe(1)–C(2)	1.76(4)	Fe(2)–C(5)	1.77(3)	Fe(3)–C(8)	1.80(3)
	Fe(1)–C(3)	1.64(5)	Fe(2)–C(6)	1.81(3)	Fe(3)–C(9)	1.81(4)
C–O	C(1)–O(1)	1.17(4)	C(4)–O(4)	1.11(4)	C(7)–O(7)	1.20(5)
	C(2)–O(2)	1.15(5)	C(5)–O(5)	1.21(4)	C(8)–O(8)	1.11(4)
	C(3)–O(3)	1.24(6)	C(6)–O(6)	1.12(4)	C(9)–O(9)	1.16(4)
Au–Au–Au	Au(1)–Au(2)–Au(3)	60.05(5)	Au(1)–Au(3)–Au(2)	61.17(5)	Au(2)–Au(1)–Au(3)	58.78(5)
Fe–Fe–Fe	Fe(1)–Fe(2)–Fe(3)	60.0(2)	Fe(2)–Fe(1)–Fe(3)	60.3(2)	Fe(1)–Fe(3)–Fe(2)	59.8(2)
Au–Fe–Fe	Au(3)–Fe(1)–Fe(3)	106.3(2)	Au(2)–Fe(2)–Fe(1)	111.3(2)	Au(2)–Fe(2)–Fe(3)	92.7(2)
	Au(3)–Fe(2)–Fe(1)	60.0(2)	Au(3)–Fe(2)–Fe(3)	104.4(2)	Au(3)–Fe(1)–Fe(2)	62.3(2)
Fe–Au–Fe	Fe(1)–Au(3)–Fe(2)	57.7(2)				
Au–Fe–Au	Au(2)–Fe(2)–Au(3)	71.2(1)				
Au–Au–Fe	Au(1)–Au(2)–Fe(2)	96.1(1)	Au(1)–Au(3)–Fe(2)	94.7(1)	Au(2)–Au(3)–Fe(2)	52.8(1)
	Au(1)–Au(3)–Fe(1)	85.7(1)	Au(3)–Au(2)–Fe(2)	56.0(1)	Au(2)–Au(3)–Fe(1)	96.2(1)
Au–Au–P	Au(1)–Au(2)–P_c	45.3(2)	Au(2)–Au(1)–P_c	49.0(2)	Au(3)–Au(1)–P_c	50.8(2)
	Au(1)–Au(2)–P(2)	119.1(2)	Au(2)–Au(1)–P(1)	140.1(3)	Au(3)–Au(1)–P(1)	129.9(2)
	Au(1)–Au(3)–P_c	45.8(2)	Au(2)–Au(3)–P_c	49.6(2)	Au(3)–Au(2)–P_c	50.9(2)
	Au(1)–Au(3)–P(3)	111.2(2)	Au(2)–Au(3)–P(3)	126.2(2)	Au(3)–Au(2)–P(2)	141.6(2)
Fe–Fe–P	Fe(1)–Fe(2)–P_c	55.4(3)	Fe(2)–Fe(1)–P_c	54.9(3)	Fe(3)–Fe(1)–P_c	51.5(3)
	Fe(1)–Fe(3)–P_c	56.4(3)	Fe(2)–Fe(3)–P_c	55.9(3)	Fe(3)–Fe(2)–P_c	51.5(3)
Fe–Fe–C	Fe(1)–Fe(2)–C(4)	137(1)	Fe(2)–Fe(1)–C(1)	102(1)	Fe(3)–Fe(1)–C(1)	157(1)
	Fe(1)–Fe(2)–C(5)	123(1)	Fe(2)–Fe(1)–C(2)	143(2)	Fe(3)–Fe(1)–C(2)	105(1)
	Fe(1)–Fe(2)–C(6)	67(1)	Fe(2)–Fe(1)–C(3)	112(2)	Fe(3)–Fe(1)–C(3)	81(2)
	Fe(1)–Fe(3)–C(7)	95(1)	Fe(2)–Fe(3)–C(7)	151(1)	Fe(3)–Fe(2)–C(4)	82(1)
	Fe(1)–Fe(3)–C(8)	154(1)	Fe(2)–Fe(3)–C(8)	101(1)	Fe(3)–Fe(2)–C(5)	173(1)
	Fe(1)–Fe(3)–C(9)	103(1)	Fe(2)–Fe(3)–C(9)	97(1)	Fe(3)–Fe(2)–C(6)	91(1)
Fe–Au–P	Fe(1)–Au(3)–P_c	52.7(2)	Fe(2)–Au(2)–P_c	53.4(2)	Fe(2)–Au(3)–P_c	51.6(2)
	Fe(1)–Au(3)–P(3)	137.6(3)	Fe(2)–Au(2)–P(2)	144.9(3)	Fe(2)–Au(3)–P(3)	149.2(3)
Au–Fe–P	Au(2)–Fe(2)–P_c	58.7(3)	Au(3)–Fe(1)–P_c	59.0(2)	Au(3)–Fe(2)–P_c	58.2(2)
Au–Fe–C	Au(2)–Fe(2)–C(4)	87(1)	Au(3)–Fe(1)–C(1)	73(1)	Au(3)–Fe(2)–C(4)	157(1)
	Au(2)–Fe(2)–C(5)	80(1)	Au(3)–Fe(1)–C(2)	95(1)	Au(3)–Fe(2)–C(5)	74(1)
	Au(2)–Fe(2)–C(6)	175(1)	Au(3)–Fe(1)–C(3)	165(2)	Au(3)–Fe(2)–C(6)	105(1)
Au–P–Au	Au(1)–P_c–Au(2)	85.7(3)	Au(1)–P_c–Au(3)	83.5(3)	Au(2)–P_c–Au(3)	79.4(2)
Fe–P–Fe	Fe(1)–P_c–Fe(2)	69.7(3)	Fe(1)–P_c–Fe(3)	72.1(3)	Fe(2)–P_c–Fe(3)	72.6(3)
Au–P–Fe	Au(1)–P_c–Fe(1)	121.4(4)	Au(2)–P_c–Fe(1)	133.3(4)	Au(3)–P_c–Fe(1)	68.3(3)
	Au(1)–P_c–Fe(2)	145.4(4)	Au(2)–P_c–Fe(2)	68.0(3)	Au(3)–P_c–Fe(2)	70.3(3)
	Au(1)–P_c–Fe(3)	140.7(4)	Au(2)–P_c–Fe(3)	112.2(4)	Au(3)–P_c–Fe(3)	132.7(4)
Au–P–C	Au(1)–P(1)–C(111)	113(2)	Au(2)–P(2)–C(211)	110.5(8)	Au(3)–P(3)–C(311)	116.6(7)
	Au(1)–P(1)–C(121)	115.5(8)	Au(2)–P(2)–C(221)	113.3(8)	Au(3)–P(3)–C(321)	112.0(8)
	Au(1)–P(1)–C(131)	115(1)	Au(2)–P(2)–C(231)	114.4(9)	Au(3)–P(3)–C(331)	111.2(7)
	Au(1)–P(1)–C(141)	115.3(4)				
	Au(1)–P(1)–C(151)	112.7(5)				
P–Au–P	P_c–Au(1)–P(1)	170.9(3)	P_c–Au(2)–P(2)	158.5(3)	P_c–Au(3)–P(3)	157.0(3)
P–Fe–C	P_c–Fe(1)–C(1)	132(1)	P_c–Fe(2)–C(4)	115(1)	P_c–Fe(3)–C(7)	99(1)
	P_c–Fe(1)–C(2)	89(2)	P_c–Fe(2)–C(5)	124(1)	P_c–Fe(3)–C(8)	100(1)
	P_c–Fe(1)–C(3)	132(2)	P_c–Fe(2)–C(6)	121(1)	P_c–Fe(3)–C(9)	151(1)
C–Fe–C	C(1)–Fe(1)–C(2)	98(2)	C(4)–Fe(2)–C(5)	97(2)	C(7)–Fe(3)–C(8)	98(2)
	C(1)–Fe(1)–C(3)	95(2)	C(4)–Fe(2)–C(6)	97(2)	C(7)–Fe(3)–C(9)	103(2)
	C(2)–Fe(1)–C(3)	96(2)	C(5)–Fe(2)–C(6)	97(2)	C(8)–Fe(3)–C(9)	96(2)
Fe–C–O	Fe(1)–C(1)–O(1)	173(3)	Fe(2)–C(4)–O(4)	176(3)	Fe(3)–C(7)–O(7)	172(4)
	Fe(1)–C(2)–O(2)	176(4)	Fe(2)–C(5)–O(5)	173(3)	Fe(3)–C(8)–O(8)	172(3)
	Fe(1)–C(3)–O(3)	175(4)	Fe(2)–C(6)–O(6)	166(3)	Fe(3)–C(9)–O(9)	174(3)

[a] Estimated standard deviations in the least significant digit(s) are given in parentheses.

the second between the third gold fragment, which caps the Fe_h–Fe_w–B face, and one of the Fe_w–B-edge-bridging fragments. The fact that only two Au···Au bonds are observed for the Au_3–borane cluster may be a result of steric crowding from the additional $Fe(CO)_3$ fragment.

Low-Temperature ^{31}P NMR Spectroscopy. Each phosphine ligand is in a unique coordination environment in the clusters Au_2-**4a** and Au_3-**5a** in the solid state, although a single phosphine environment is observed by ^{31}P NMR spectroscopy at room temperature for **4a,b** and **5a,b** as described above. It is clear that an *intramolecular* process is operative in equilibrating the gold-bound phosphine ligands since coupling between the cluster-bound phosphorus atom (P_c) and the phosphine ligands is maintained. Low-temperature ^{31}P NMR spectroscopy was performed to attempt to reconcile the ^{31}P NMR spectra and the solid-state structures. Selected variable-temperature $^{31}P\{^1H\}$ NMR spectra for **4a** from room temperature to 170 K are shown in Figure 4. Upon lowering of the temperature to 170 K, the doublet observed in the phosphine region at room temperature collapses to the baseline and resharpens as two doublets with distinctly different couplings to P_c. The upfield resonance with a large $^2J_{PP}$ value of 290 Hz is assigned to the $(R_3P)Au^+$ fragment bound to the cluster exclusively through P_c (Au(1)) on the basis of the similarity of the $^2J_{PP}$ value to that observed for the monosubstituted cluster (for **3a**, $^2J_{PP}$ = 314 Hz). The downfield doublet ($^2J_{PP}$ = 98 Hz) is assigned to the $(R_3P)Au^+$ fragment that bridges the Fe–P edge (Au(2)). No coupling is observed between the gold-bound phosphine ligands. In the P_c region of the spectrum, the central resonance of the triplet observed at room temperature collapses and resharpens as two distinct resonances to yield a doublet of

Table VIII. Low-Temperature $^{31}P\{^1H\}$ NMR Data for Au-Substituted Clusters[a]

compd	T, K	$\delta(\mu_3\text{-P})$	$\delta(PR_3)$	$^2J_{PP}$
$(\mu\text{-H})Fe_3(CO)_9P[Au(PPh_3)]_2$ (**4a**)[b]	170	253.2 (dd)	47.7 (d)	98
			40.1 (d)	290
$(\mu\text{-H})Fe_3(CO)_9P[Au(PEt_3)]_2$ (**4b**)[b]	170	267.7 (dd)	52.5 (d)	97
			44.3 (d)	286
$(\mu\text{-H})Fe_3(CO)_9P\{[Au(PPh_3)][Au(PEt_3)]\}$ (**4c**)[b]	170	266.1 (dd)		91, 293[d]
		263.7 (dd)		94, 296[d]
$Fe_3(CO)_9P[Au(PPh_3)]_3$ (**5a**)[c]	138	114.4 (br)	44.2 (br)	
$(\mu\text{-H})_2Fe_3(CO)_9P[Au(PPh_3)_2]$ (**3a**·PPh_3)[b]	170	448.0 (t)	42.5 (d)	152
$(\mu\text{-H})Fe_3(CO)_9P\{[Au(PPh_3)_2][Au(PPh_3)]\}$ (**4a**·PPh_3)[b]	170	298.5 (dt)	46.1 (d)	112, 1P, $Au(PPh_3)$
			43.5 (d)	122, 2P, $Au(PPh_3)_2$

[a] δ reported in ppm and J reported in Hz. [b] CD_2Cl_2. [c] 1:1 $CD_2Cl_2/CHFCl_2$. [d] Due to severely overlapping resonances, it is difficult to make specific assignments of phosphine ligand resonances.

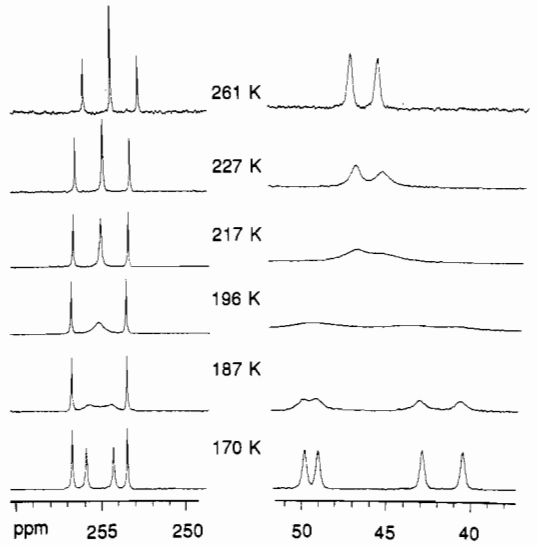

Figure 4. Variable-temperature $^{31}P\{^1H\}$ NMR spectra of $HFe_3(CO)_9P[Au(PPh_3)]_2$ (**4a**) in CD_2Cl_2.

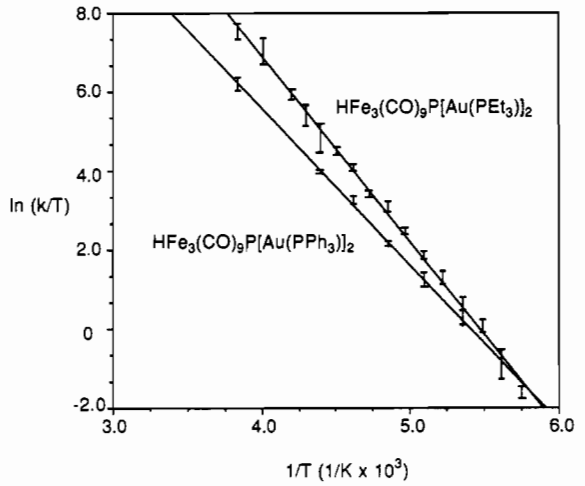

Figure 5. Plots of ln (k/T) vs $1/T$ $(1/K \times 10^3)$ for **4a,b**.

doublets at the low-temperature limit. The outer resonances remain sharp throughout the temperature range because they are separated by $J_{P1} + J_{P2}$ in both the fast- and slow-exchange regimes. The fact that the low-temperature coupling constants average to the high-temperature value indicates that there is not a change in the binding mode of the Au_2 ligand with temperature. In contrast, the PPh_3 and P_c resonances for the Au_3 cluster, **5a**, have only just begun to broaden at 143 K; thus, no additional information is available. Complete low-temperature ^{31}P NMR data are compiled in Table VIII.

For the asymmetric cluster, **4c**, the couplings between P_c and the PPh_3 (J_{PP} = 192 Hz) and PEt_3 (J_{PP} = 198 Hz) ligands are nearly equal at room temperature, indicating essentially equal population of both phosphine ligands in each of the two distinct sites. In the fast-exchange regime, differences in average population would be reflected in a larger coupling constant for the phosphine ligand preferring the large J_{PP} site (and a smaller coupling constant for the phosphine ligand preferring the small J_{PP} site) because of the large difference in the values of the coupling constants observed for the two distinct sites. At low temperature, two distinct P_c resonances are observed for **4c** in the ^{31}P NMR spectrum corresponding to isomers with PEt_3 and PPh_3 bound in the large J_{PP} site in a ~1:1 ratio.

Rates of the fluxional process that equilibrates the two gold-bound phosphine ligands in the Au_2 clusters can be conveniently measured by fitting the variable-temperature NMR data using the program DNMR3.[12] Eyring plots of the data for **4a,b** over a 55-deg temperature range are presented in Figure 5, and the resulting activation parameters are collected in Table IX. The observed ΔS^* values for **4a,b** are near zero, consistent with an intramolecular rearrangement. The free energies of activation, ΔG^*, at 298 K are very similar for **4a** (9.2 kcal mol^{-1}) and **4b** (8.2 kcal mol^{-1}), indicating that the energetics of the fluxional process are relatively insensitive to the identity of the PR_3 substituent on gold. Two additional experiments were performed to gain further insight into the fluxional process. The influence of the cluster-bound hydrogen ligand on the dynamics can be probed by deprotonating **4a** with dbu (dbu = 1,8-diazabicyclo[5.4.0]undec-7-ene). The deprotonation reaction does not proceed cleanly, and formation of the Au_3 cluster, **5a**, is observed in addition to unidentified decomposition products; however, the deprotonated product, $[Fe_3(CO)_9P\{Au(PPh_3)\}_2]^-$, is identified in the 170 K ^{31}P NMR spectrum as a sharp triplet at δ 224.7 ppm ($^2J_{PP}$ = 176 Hz). Thus, the activation barrier for the fluxional process equilibrating the gold-bound phosphine ligands must be lower in $[Fe_3(CO)_9P\{Au(PPh_3)\}_2]^-$ than in **4a**. A ^{13}C NMR experiment, which should also be sensitive to rearrangement of the Fe_3PAu_2 core, was also performed. At room temperature, a single ^{13}C resonance is observed for all of the CO ligands. As the temperature is lowered, the singlet collapses, and a 213 K, a broadened 3:6 pattern of resonances is observed. At 183 K, a 1:2:2:2:2 pattern of resonances, consistent with the solid-state structure for **4a**, sharpens (Table X). For a singlet to be observed in the ^{13}C NMR spectrum at room temperature, the hydride position is likely delocalized on the Fe_3 frame.[18]

Table IX. Activation Parameters for the Fluxional Process Observed for Au_2 Clusters[a]

compd	ΔG^*, kcal mol^{-1} [b]	ΔH^*, kcal mol^{-1}	ΔS^*, cal mol^{-1} K^{-1}
$(\mu\text{-H})Fe_3(CO)_9P[Au(PPh_3)]_2$ (**4a**)	9.2	7.9(1)	−4.5(6)
$(\mu\text{-H})Fe_3(CO)_9P[Au(PEt_3)]_2$ (**4b**)	8.2	9.4(1)	4.0(6)

[a] Error estimates for the linear regressed parameters were obtained by following the approach outlined by: Sandström, J., *Dynamic NMR Spectroscopy*; Academic Press, Inc.: New York, 1982. [b] At 298 K.

Dynamic processes that equilibrate two or more unique $M(PR_3)$ units bound to metal carbonyl clusters are commonly observed.[19]

Table X. $^{13}C\{^1H\}$ NMR Data for the CO Ligands in $(\mu\text{-H})Fe_3(CO)_9P[Au(PR_3)]_2$ Clusters[a]

compd	T, K	δ(CO), ppm
$(\mu\text{-H})Fe_3(CO)_9P[Au(PPh_3)]_2$ (**4a**)[b]	293	214.5, s
	193	209.6 (c), 2C; 213.3 (d), 2C; 214.6 (a), 2C; 216.9 (b), 2C; 225.5 (e), 1C
$(\mu\text{-H})Fe_3(CO)_9P[Au(PEt_3)]_2$ (**4b**)[c]	293	215.0, s
	193	217.8, (d, e), 3C; 213.2, (a, b, c), 6C
	173	209.9 (c), 2C; 213.6 (d), 2C; 215.1 (a), 2C; 217.4 (b), 2C; 226.1 (e), 1C

[a] Assignments of δ(CO) based on **I**. [b] 1:1 CH_2Cl_2/CD_2Cl_2. [c] CD_2Cl_2.

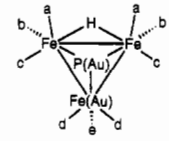

I

Direct evidence has been obtained from indirectly-detected $^{109}Ag\{^1H\}$ NMR spectroscopy which establishes that rearrangement of the heterometal cores is responsible for the observed equilibration of the two unique Ag sites in the clusters $(\mu_3\text{-H})_2Ru_4(CO)_{12}[Ag_2(\mu\text{-}Ph_2P(CH_2)_nPPh_2)]$.[20] Assuming that rearrangement of the heterometal cores is responsible for the observed fluxional behavior in Au_2 clusters above, a consistent picture emerges to explain the data. In the core of **4a**, the interaction of the $Au_2(PR_3)_2$ fragment will be the strongest with the Fe atom that does not interact with the hydride ligand. The hydride ligand apparently plays a role in freezing out the fluxionality in **4a** since the deprotonated cluster remains fluxional at 173 K. Accordingly, a mechanism is proposed where movement of the Au_2 unit on the Fe_3P frame, which is associated with movement of the hydride ligand, interchanges P_A and P_B (eq 2).

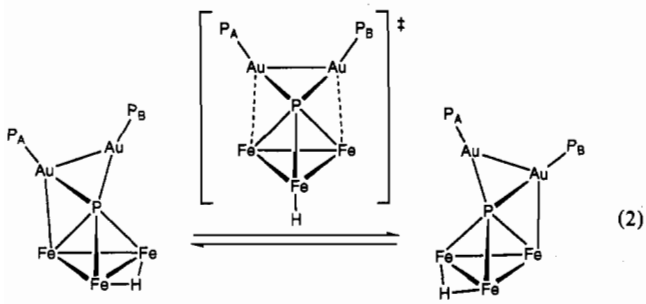

(2)

Phosphine Addition Reactions. The coupling to the cluster-bound phosphorus atom (P_c) serves as a probe of ligand addition reactions at the gold sites in addition to the dynamics of the gold–phosphine units. Upon addition of 2 equiv of PPh_3 to the monogold cluster, **3a**, coupling is lost between P_c and the PPh_3 ligand, indicating exchange of free and gold-bound PPh_3, and the chemical shift of P_c moves ~30 ppm downfield. A single broad resonance is observed for free and bound PPh_3. At 170 K, a broad triplet is observed in the ^{31}P NMR spectrum for P_c at δ 448.0 ppm ($^2J_{PP}$ = 152 Hz), 30 ppm further downfield than at room temperature, with a corresponding doublet in the phosphine region at δ 42.5 ppm, clearly demonstrating a low-temperature product with two phosphine ligands bound to gold (**3a**·PPh_3, Scheme I). Exchange between **3a** and **3a**·PPh_3 is rapid at room temperature, and the chemical shift for the single P_c resonance reflects the relative amounts of **3a** and **3a**·PPh_3. Over the course of the experiment, the sample degrades and other cluster products are observed. The addition of an excess of the more basic phosphine ligand PEt_3 results in clean extrusion of the Au^+ fragment from the cluster producing $[(\mu\text{-H})Fe_3(CO)_9(\mu_3\text{-PH})]^-$ as the cluster product.

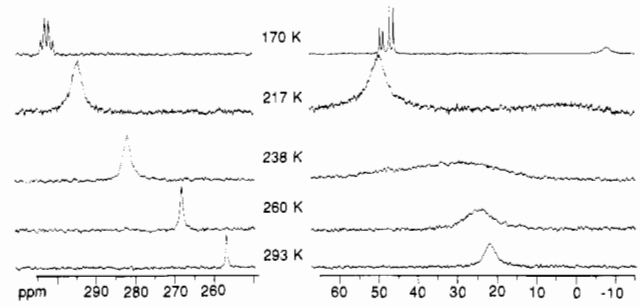

Figure 6. Variable-temperature $^{31}P\{^1H\}$ NMR spectra for $HFe_3(CO)_9P[Au(PPh_3)]_2$ and 2 equiv of PPh_3 in CD_2Cl_2.

Observation of the reaction between **3a** and PPh_3 prompted the investigation of the reaction of **4a** and **5a** with free PPh_3. The Au_2 cluster, **4a**, also coordinates 1 equiv of PPh_3 at low temperature as demonstrated by ^{31}P NMR spectroscopy. The broad room-temperature singlet for P_c at δ 257 ppm in the presence of 2 equiv of PPh_3 is cleanly replaced by an overlapping triplet of doublets centered at δ 298.5 ppm ($^2J_{PP}$ = 122 Hz, $^2J_{PP}$ = 112 Hz) at 170 K, assigned to a cluster with a coordinated $Au_2(PPh_3)_3$ unit (**4a**·PPh_3, Scheme I). In the phosphine region of the spectrum, the broad room-temperature singlet for free and bound PPh_3 is replaced by two doublets, in a 2:1 ratio, and a separate resonance for free PPh_3 at 170 K. The gold(I) fragment bound to two phosphine ligands is assigned to the complex that is bound to the cluster only through P_c. The Au_3 cluster, **5a**, exchanges with free PPh_3 more slowly than **4a** under identical conditions, and in the phosphine region of the room-temperature spectrum, broad but distinct resonances are observed for free and gold-bound PPh_3, and no PPh_3 coupling to P_c is observed. At low temperature, coupling is observed again between P_c and the coordinated PPh_3 ligands; however, no new resonances are observed corresponding to a PPh_3 adduct. Formation of the Au_3 triangle, which increases the coordination number of the apically-bound gold fragment by one, must result in effective coordinative saturation of all gold(I) fragments.

A single P_c resonance that shifts progressively downfield at lower temperatures is observed for **4a** in the presence of 2 equiv of PPh_3 down to 208 K (see Figure 6), indicating exchange between the original cluster and the phosphine adduct is rapid on the time scale determined by the frequency difference between **4a** and **4a**·PPh_3; as above for **3a**, the chemical shift for P_c reflects the relative amount of each complex. The clean reaction of **4a** with PPh_3 permitted evaluation of the equilibrium constant for PPh_3 addition to **4a** as a function of temperature using variable-temperature $^{31}P\{^1H\}$ NMR spectroscopy. From the temperature dependence of the chemical shift for P_c, the amount of **4a** and **4a**·PPh_3 at each temperature can be extracted, enabling calculation of the equilibrium constant (see Experimental Section). At 293

(18) Because the hydride ligand adopts a ground-state bridging structure, it seems more likely that the hydride ligand is mobile instead of the alternate explanation of triangle-delocalized exchange of CO ligands.
(19) (a) Salter, I. D. *Adv. Dyn. Stereochem.* **1988**, *2*, 57. (b) Orpen, A. G.; Salter, I. D. *Organometallics* **1991**, *10*, 111.
(20) Brown, S. S. D.; Colquhoun, I. J.; McFarlane, W.; Murray, M.; Salter, I. D.; Sik, V. *J. Chem. Soc., Chem. Commun.* **1986**, 53.

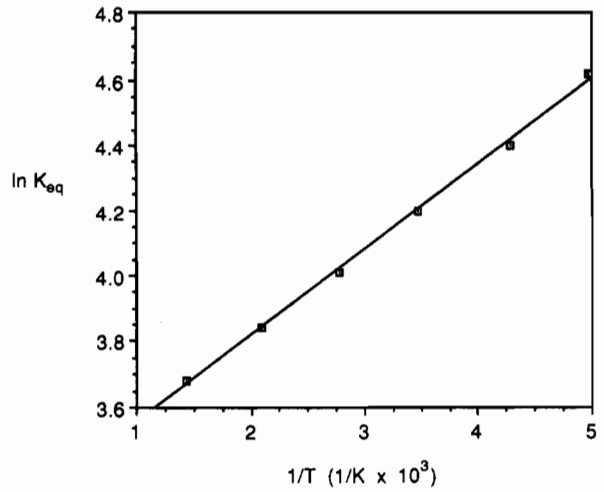

Figure 7. Plot of ln K_{eq} vs $1/T$ ($1/K \times 10^3$) for PPh_3 addition to **4a**.

K, 93% of the cluster exists as **4a**, while at 217 K, 84% of the cluster exists as **4a**·PPh_3. A plot of ln K_{eq} versus $1/T$ over a 55-deg temperature range using data that contain at least 20% each of **4a** and **4a**·PPh_3 is linear (Figure 7). Analysis of the slope and intercept of the plot yields $\Delta H° = -7.6(2)$ kcal mol^{-1} and $\Delta S° = -25.0(7)$ cal mol^{-1} K^{-1} for addition of PPh_3 to **4a**. The dramatic temperature dependence of the equilibrium constant for the phosphine addition reaction results from the large negative entropic contribution to the free energy coupled with the relatively small negative enthalpic contribution to the free energy.

Conclusions. The high affinity of the cluster-bound phosphorus atom for Au(I) fragments as well as the Au···Au interactions between the formally d^{10} Au(I) fragments are the driving forces in determining the structures of the gold-substituted derivatives of the cluster $[(H)_nFe_3(CO)_9P]^{(3-n)-}$. The initial $P[Au(PPh_3)]$ interaction in the terminal position on the cluster-bound phosphorus atom serves as a nucleation site for the assembly of Au_2 and triangular-Au_3 arrays, where each gold(I) fragment is in a unique coordination environment on the Fe_3P cluster frame.[21] The presence of the cluster-bound phosphorus atom provides a sensitive NMR probe for the dynamics of the $(H)_n$-$Fe_3(CO)_9P[Au(PPh_3)]_{3-n}$ clusters, where a single phosphine ligand environment is observed at room temperature for the Au_2 and Au_3 clusters. The PPh_3 addition reactions that occur at low temperature to the apical gold sites in the Au_1 and Au_2 clusters can also be probed by ^{31}P NMR spectroscopy, and the fact that these reactions take place indicates that the $(Ph_3P)Au^+$ fragment bound to the cluster only through P_c is effectively coordinatively unsaturated until a triangular-Au_3 array is formed. The binding modes of fragments that prefer a μ_3-coordination mode on the $[(H)_nFe_3(CO)_9P]^{(3-n)-}$ frame are currently under investigation.

Acknowledgment. Partial financial support was provided by a Presidential Young Investigator Award from the National Science Foundation (Grant CHEM-8958027). Partial funds for equipping the single-crystal X-ray diffraction facility at UNC-CH were provided by the National Science Foundation (Grant CHE-8919288). D.L.S. was supported, in part, by a fellowship from the Department of Education. Dr. David L. Harris is acknowledged for initial assistance with spectral fits using the program DNMR3.

Supplementary Material Available: Crystallographic results for **4a** and **5a** not appearing in the printed paper, including tables of crystallographic parameters, fractional atomic coordinates, bond lengths and angles, and anisotropic thermal parameters (11 pages). Ordering information is given on any current masthead page.

(21) After submission of this work, we were successful in isolating the cationic cluster, $[Fe_3(CO)_9P\{Au(PPh_3)\}_4]^+$, where the Au_4 array adopts a nearly square-planar arrangement: Sunick, D. L.; White, P. S.; Schauer, C. K. *Angew. Chem.*, in press.